

A systematic RNAi synthetic interaction screen reveals a link between p53 and snoRNP assembly

Dragomir B. Krastev^{1,2}, Mikolaj Slabicki², Maciej Paszkowski-Rogacz^{1,2}, Nina C. Hubner^{3,4}, Magno Junqueira^{2,4}, Andrej Shevchenko², Matthias Mann³, Karla M. Neugebauer² and Frank Buchholz^{1,2,5}

TP53 (tumour protein 53) is one of the most frequently mutated genes in human cancer and its role during cellular transformation has been studied extensively. However, the homeostatic functions of p53 are less well understood. Here, we explore the molecular dependency network of *TP53* through an RNAi-mediated synthetic interaction screen employing two HCT116 isogenic cell lines and a genome-scale endoribonuclease-prepared short interfering RNA library. We identify a variety of *TP53* synthetic interactions unmasking the complex connections of p53 to cellular physiology and growth control. Molecular dissection of the *TP53* synthetic interaction with *UNRIP* indicates an enhanced dependency of *TP53*-negative cells on small nucleolar ribonucleoprotein (snoRNP) assembly. This dependency is mediated by the snoRNP chaperone gene *NOLC1* (also known as *NOPP140*), which we identify as a physiological p53 target gene. This unanticipated function of *TP53* in snoRNP assembly highlights the potential of RNAi-mediated synthetic interaction screens to dissect molecular pathways of tumour suppressor genes.

More than 30 years of intense research on the tumour suppressor gene *TP53* has revealed its relevance in many aspects of tumour biology (reviewed in ref. 1). It is now well established that p53 (the protein product of *TP53*) activation leads to the execution of a complex genetic program that limits cellular proliferation and leads to senescence or apoptosis^{2,3}. Several lines of evidence have pointed to an under-appreciated homeostasis function of p53 in normal, unstressed cells⁴. As a transcription factor, p53 can mediate the expression levels of its target genes, thereby adjusting cellular homeostasis of basic metabolism⁵, balance of reactive oxygen species^{6,7}, stem cell identity and reprogramming⁸ and animal reproduction⁹. These data establish an important role for p53 in cellular homeostasis and indicate that p53-loss-of-function cells become genetically rewired in a way that discriminates them from wild-type cells, a premise that could be explored for the identification of possible p53 genetic dependencies.

Synthetic interaction screens have led the way in identifying new and unanticipated functional interactions between seemingly unrelated protein complexes in yeast^{10,11}. In mammalian cells, RNA interference (RNAi)-based synthetic interaction screens are a promising approach to dissect genetic dependencies and the first studies on mammalian synthetic interactions of oncogenes have demonstrated the power of this approach^{12,13}. Furthermore, synthetic lethal screens have identified genes that sensitize cells

to different chemical drugs^{14,15}. Several synthetic interactions with tumour suppressor genes have also been published^{11,16}, but to our knowledge a genome-scale survey for synthetic interactions of a tumour suppressor gene has not been reported. Here, we present the results of a systematic investigation of *TP53* genetic dependencies and characterize in molecular detail a homeostatic function of p53 in snoRNP biogenesis.

RESULTS

Genome-scale synthetic interaction RNAi screen with *TP53*

We carried out a genome-scale RNAi screen in two HCT116 cell lines that differ only in their *TP53* status: *TP53* wild type and its *TP53*-knockout counterpart (ref. 17). The wild-type cells show a robust p53-dependent response and both lines allow efficient transcript depletion through RNAi (Supplementary Fig. S1a–c). An endoribonuclease-prepared short interfering RNA (esiRNA) library was used to interrogate which genes are needed for proliferation of either cell type and thus discriminate the specific genetic requirement of each gene in accordance with the presence or absence of *TP53*. Two major features were implemented into the screen design. First, the cells were labelled with fluorescent proteins (nuclear monomeric red fluorescent protein, mRFP, for the wild-type and green fluorescent protein, GFP, for the knockout cells), which allowed

¹University of Technology Dresden, University Hospital and Medical Faculty Carl Gustav Carus, Department of Medical Systems Biology, Fetscherstraße 74, D-01307 Dresden, Germany. ²Max Planck Institute of Molecular Cell Biology and Genetics, Pfotenhauerstrasse 108, D-01307 Dresden, Germany. ³Max Planck Institute of Biochemistry, Am Klopferspitz 18, 82152 Martinsried, Germany. ⁴Present addresses: Universitair Medisch Centrum Utrecht, 3508 AB Utrecht, The Netherlands (N.C.H.); Brazilian Center for Protein Research, Department of Cell Biology, University of Brasilia, 70910-900 Brasilia, DF, Brazil (M.J.).

⁵Correspondence should be addressed to F.B. (e-mail: buchholz@mpi-cbg.de)

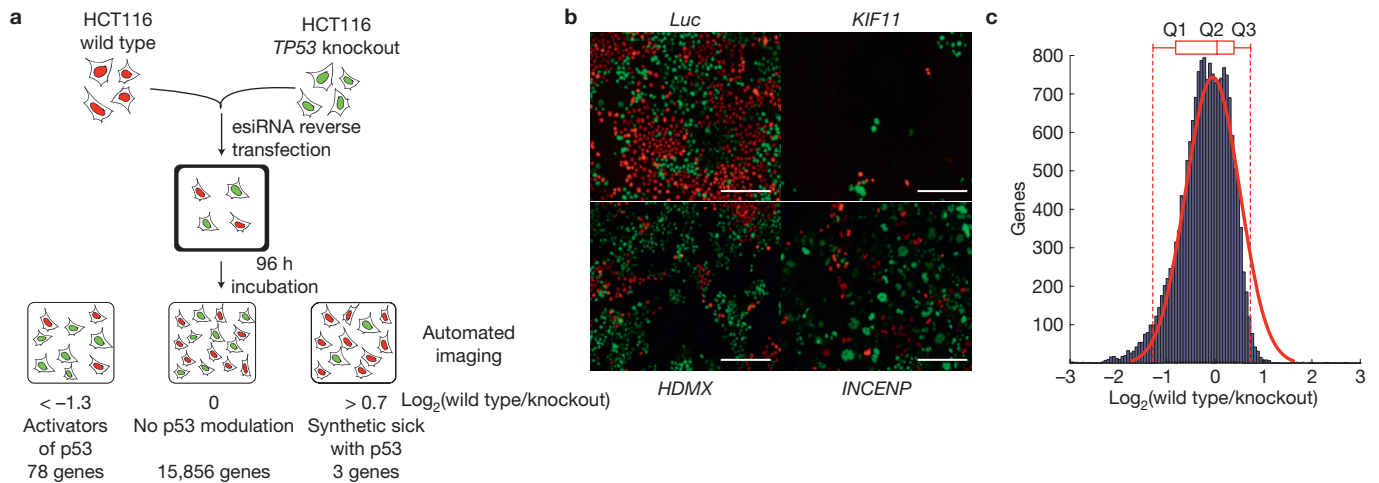


Figure 1 Genome-scale *TP53* synthetic interaction screen. (a) Schematic representation of the screen assay. Equal numbers of HCT116 wild-type (red) and knockout (green) cells were reverse transfected with esiRNAs. Possible scenarios and the number of knockdowns causing indicated phenotypes are shown. Screen controls are shown in Supplementary Fig. S1a–c. (b) Representative images from transfections with esiRNAs of the non-targeting luciferase control (*Luc*), the kinesin family member 11 (*KIF11*), the p53 regulator

HDMX and the inner centromere protein antigens 135/155 kDa (*INCENP*) exemplifying knockdown phenotypes (scale bars, 100 μm). (c) Statistical evaluation of the screening results. A histogram of the $\text{log}_2(\text{wildtype/knockout})$ calculated in a plate-wise manner is shown. The Gaussian fit to the distribution (red line) underlines the need to use an asymmetry- and outlier-insensitive quartile (Q)-based threshold (dashed lines, see Methods) with a targeted error rate of 0.05 to determine the primary hits.

a microscopy-based readout at single-cell resolution. Second, the wild-type and knockout cells were mixed in a 1:1 ratio and transfected with esiRNAs in the same well, ensuring that their viability is compared under precisely the same conditions, reducing the technical variability and significantly improving the identification of genetic interactions (Fig. 1a). The robustness of the assay was first evaluated by treatment with Nutlin-3 α (ref. 18) or *HDMX* depletion¹⁹. As expected, both treatments triggered a p53 response and led to significant retardation of proliferation of the wild-type, but not the knockout, cells, thus changing the starting ratio of 1:1 to 0.1:1 in favour of the knockout cells (Supplementary Fig. S1a–c). Depletion of essential genes, such as kinesin family member 11 (*KIF11*), equally affected wild-type and knockout cells (Fig. 1b), excluding the possibility that one cell line is more sensitive to the transfection protocol. Thus, the assay is amenable for a high-throughput RNAi screen and the wild-type/knockout ratio is a robust readout of p53 activation.

The esiRNA library was transfected in duplicate and automated image analysis was used to extract the numbers of wild-type and knockout cells at 96 h post-transfection^{20–22} (Fig. 1a–c and Supplementary Table S1). A total of 780 (4.8%) knockdowns affected the cell viability of both cells types, with 276 (1.7%) leading to overall cell counts that prohibited meaningful analyses of altered wild-type/knockout ratios (Supplementary Table S1, viability column). Reactome²³ and STRING (ref. 24) database analyses revealed that genes encoding core proteins of complexes involved in cell cycle progression, general transcription, messenger RNA processing and protein translation (for example, almost all core subunits of the ribosome, Table 1) were highly enriched in reduced-viability phenotypes in both cell lines. These genes therefore represent the molecular machineries that drive basic cellular proliferation and were excluded from further analysis.

Using an outlier- and asymmetry-insensitive quartile-based technique²⁵ to identify primary hits, followed by stringent validation, we identified 81 knockdowns that led to viability phenotypes in

only one of the two cell types (Supplementary Table S2). Depletion of 78 genes specifically decreased proliferation and/or viability of the wild-type cells with little to no effect on the knockout cells. These genes represent the genetic interaction network that specifically synergize with *TP53* and represent the multitude of pathways that p53 monitors or regulates under normal growth conditions. Interestingly, many of the 78 hit genes that reduced the wild-type/knockout ratio are also involved in basic cellular processes, but not as core components. For example, the depletion of a number of genes encoding ribosome assembly and ribosome maturation factors, such as *PES1* (pescadillo homologue 1, containing BRCT domain), *RRS1* (RRS1 ribosome biogenesis regulator homologue) and *RPF1* (ribosome production factor 1 homologue), decreased the wild-type/knockout ratio (Table 1). These genes are positioned upstream of the mature ribosome subunits that are known to activate the ribosomal protein (RP)–Hdm2–p53 pathway (reviewed in ref. 26), but downstream of the ribosomal RNA transcription machinery. There are more than 170 ribosome assembly factors²⁷ and the finding that only a small number of them induce p53 in our screen indicates that p53 monitors specific steps in the assembly process. Interference with their functions propagates signalling through the p53 pathway, explaining the wild-type-specific phenotype. Therefore, the genes that decreased the wild-type/knockout ratio can be termed activators of p53. They have roles in cellular processes that are guarded by p53 under normal growth conditions and probably act as p53 cell stress sensors in basic cellular processes.

Knockdowns that selectively affect *TP53*-knockout cells

The fact that many more knockdowns specifically affected the wild-type cells underscores the crucial role of p53 as a guardian of cell proliferation. However, examination of the screening results also revealed three genes that increased the wild-type/knockout ratio. Knockdown of *UNRIP* (also known as *STRAP*, serine/threonine

Table 1 Phenotypes observed for core ribosome and ribosome assembly factors.

	Ribosome (mature ribosome)	Ribosome assembly factors
Phenotype	Viability	Decreased wild-type/knockout ratio
Wild-type cells	Cell death	Reduced viability
Knockout cells	Cell death	Viable
Genes	<i>RPL3, RPL5, RPL6, RPL7, RPL7A, RPL9, RPL11, RPL17, RPL18, RPL18A, RPL21, RPL23, RPL24, RPL30, RPL31, RPL32, RPL37, RPL37A, RPSA, RPS3, RPS3A, RPS4X, RPS6, RPS7, RPS8, RPS10, RPS11, RPS12, RPS15A, RPS16, RPS19, RPS20, RPS26, RPS27A</i>	<i>PES1, RRS1, UTP15, NOP2, RPF1, FBL, MRM1, RPL24, NSA2, RPL35A, GTPBP4, EBNA1BP2, ISG20L2, POLR1A, TWISTNB</i>
Enrichment (<i>P</i> value)	1.8×10^{-44}	3.9×10^{-9}

Gene Ontology term enrichment of the two groups of genes in the viability list and the list of genes decreasing the wild-type/knockout ratio, respectively, is presented by their *P* values.

kinase receptor associated protein), *MASTL* (microtubule-associated serine/threonine kinase-like) and *KIAA1344* (also known as *TXNDC16*, thioredoxin domain containing 16) had no effect on the growth of the wild-type cells, whereas expression of these genes was required for efficient growth of the knockout cells (Fig. 2a), raising the possibility that they act in conjunction with *TP53* to maintain cellular fitness. Indeed, time-lapse video microscopy revealed that for all three knockdowns the proliferation rate of the knockout cells was reduced, whereas the wild-type cells grew with similar proliferation rates as the control transfected cells (Fig. 2b). TUNEL (TdT-mediated dUTP nick end labelling) staining showed no significant increase in the level of apoptosis, further supporting that the phenotypes are caused by slower growth of the knockout cells (Supplementary Fig. S2a).

UNRIP influences the localization of the SMN complex

The knockdown of *UNRIP* was selected for further analysis because it gave the strongest phenotype and it has not been linked to p53 thus far. Two independent and non-overlapping esiRNAs efficiently depleted both *UNRIP* transcript and protein levels (Fig. 2c,d and Supplementary Fig. S2d,e). Detailed analysis of the time-lapse videos showed that the doubling time of knockout cells was extended by about 30% (36 versus 28 h in *UNRIP* versus luciferase knockdown), thus resulting in a decrease in cell number to about 70% in comparison with the wild-type cells and control-transfected knockout cells (Fig. 2b). Neither a particular cell cycle arrest, nor an increase in the number of apoptotic cells, was observed during the time-lapse analysis and on TUNEL/propidium iodide staining (Supplementary Fig. S2a,b). Furthermore, no induction of p21^{WAF1} (also known as cyclin-dependent kinase inhibitor 1) was observed in *UNRIP*-depleted knockout cells (Supplementary Fig. S2f–h).

To substantiate the synthetic effect of *TP53* and *UNRIP*, we carried out clonogenic survival and colony formation assays in isogenic cell lines. The phenotype observed in the competitive growth assay was also seen in long-term growth experiments, demonstrating that the effect can be replicated with different assays (Fig. 2e). Consistent results were seen with two independent RNAi triggers (short hairpin RNAs and esiRNA) and in an independent pair of isogenic cell lines differing solely in their *TP53* status (RKO cells)²⁸, signifying that the *TP53*–*UNRIP* synthetic interaction is reproducible and not HCT116 specific. Furthermore, *TP53* and *UNRIP* co-depletion in HCT116 wild-type cells resulted in decreased clonogenic survival, showing that their genetic interaction is not a result of a long-term adaptation to *in vitro* culturing conditions, but rather a direct genetic interaction (Supplementary Fig. S2c). Taken together, these experiments support

a cooperative role of *TP53* and *UNRIP* in the maintenance of cellular fitness and proliferation.

UNRIP has been shown to act as a negative regulator of TGFβ (transforming growth factor β) signalling²⁹. However, none of the employed assays revealed a significant change in TGFβ signalling on *UNRIP* depletion (Supplementary Fig. S2h–j).

UNRIP has also been associated with the survival of motor neurons (SMN) complex in HeLa cells³⁰. To investigate a potential association of *UNRIP* with SMN in HCT116 cells, we generated localization and affinity purification (LAP)-tagged *UNRIP* (*UNRIP*–LAP) cell lines using the TransgeneOmics approach^{31,32}. Immunoprecipitation, followed by protein interaction analyses using mass spectrometry, revealed that human as well as mouse *UNRIP*–LAP efficiently co-purified the complete SMN complex (SMN1; SIP1, survival of motor neuron protein interacting protein 1, also known as GEMIN2; DDX20, DEAD (Asp–Glu–Ala–Asp) box polypeptide 20, also known as GEMIN3; and gem (nuclear organelle)-associated proteins 4–8, GEMIN4–8) and many of its substrates (Supplementary Table S3). Thus, *UNRIP* physically interacts with SMN components and its substrates in HCT116 cells.

The SMN complex functions as an assembly chaperone mainly for the small nuclear RNPs (snRNP; ref. 33). Most SMN complex subunits, including SMN1, show a prominent accumulation in the Cajal body³⁴. Indeed, SMN1 antibody staining revealed 3–4 Cajal bodies in wild-type and knockout cells, and *UNRIP* depletion did not alter this distribution in wild-type cells (Fig. 3a). In striking contrast, *UNRIP* depletion in knockout cells led to a significant reduction in the number of SMN1-positive Cajal bodies, with roughly one-third of the cells showing no nuclear SMN1-positive staining (Fig. 3b). Virtually identical results were obtained on examination of the Gemin2 component of the SMN complex, but not the *bona fide* structural component of Cajal bodies—P80/COIL (Supplementary Fig. S3a,b). Therefore, the whole SMN complex is specifically affected on *UNRIP* depletion in knockout cells without affecting the overall Cajal body structure. Similar results were obtained with RKO cells, in which *UNRIP* depletion led to a significant decrease in the amount of nuclear SMN1 specifically in *TP53*-knockout cells (Supplementary Fig. S3c). Cross-species RNAi rescue experiments³¹ excluded possible RNAi off-target effects as a reason for this observation (Supplementary Fig. S3d). Finally, co-depletion of *TP53* and *UNRIP* led to a significant reduction of SMN1-positive Cajal bodies in the wild-type cells, demonstrating that the observed phenotype is a primary effect of the lack of both p53 and *UNRIP* (Fig. 3a,b). Hence, simultaneous loss of p53 and *UNRIP* reduces the number of SMN-complex-positive Cajal bodies.

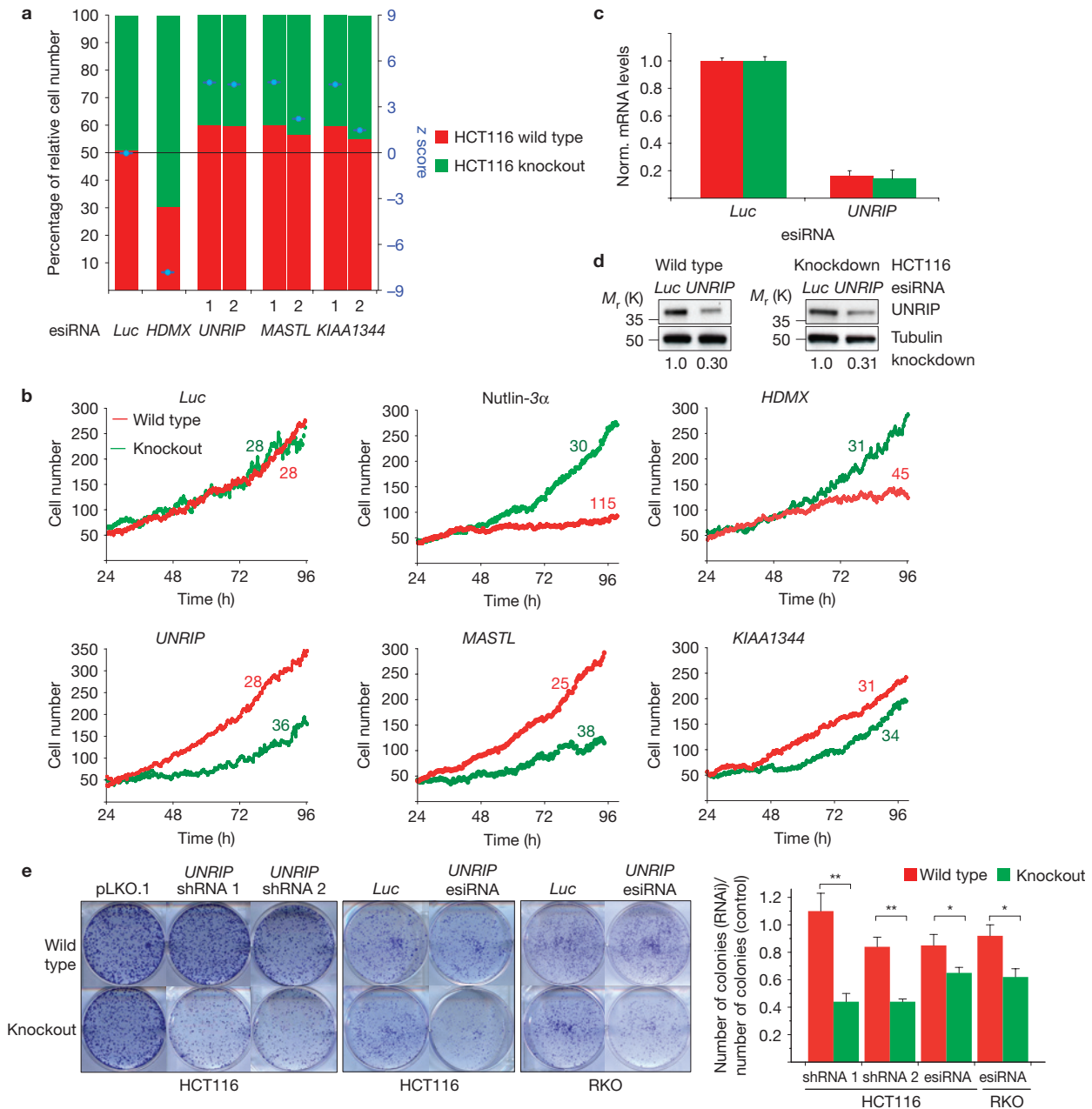


Figure 2 Depletion phenotypes of knockdowns increasing the wild-type/knockout ratio. **(a)** RNAi phenotype of the three genes decreasing the number of knockout cells—*UNRIP*, *MASTL* and *KIAA1344*. The cell number for each cell type is presented as a percentage of the total cells counted per well (left y axis) and the corresponding z score (right y axis, calculated versus *Luc* knockdown, see Methods). The knockdown of *HDMX* is shown as a positive control. Two esiRNAs (1 and 2) are shown for each hit gene. **(b)** Time-lapse analysis of the RNAi phenotypes. Wild-type and knockout cells transfected with the indicated esiRNAs were imaged for a period of 72 h, starting at 24 h post-transfection. The doubling time was calculated from an exponential fit of the growth

curves (values next to the curves). **(c,d)** Quantification of *UNRIP* knockdown. mRNA and protein depletion levels normalized to luciferase-depleted cells. GAPDH or α -tubulin served as an internal loading control (mean \pm s.d., $n = 3$). **(e)** Long-term survival (colony formation assay) of HCT116 and RKO cells on *UNRIP* depletion. The quantification presents the number of colonies relative to control transfection. The significance is determined with Student's two-tailed t -test, * P values < 0.05 , ** P values < 0.01 (mean \pm s.d., $n = 3$). The depletion phenotypes are further characterized in Supplementary Fig. S2. In all panels, red and green represent wild-type and knockout cells, respectively. Uncropped images of blots are shown in Supplementary Fig. S7a.

UNRIP influences SMN complex shuttling in a p53-dependent manner

Assembly of the Sm-ring onto the small nuclear RNA (snRNA) and the hypermethylation of the cap to trimethylguanosine (TMG) are two prerequisites for nuclear import of the newly assembled

snRNP particles to the Cajal body^{35–37}. To determine whether *UNRIP* depletion blocks cytoplasmic steps of snRNP assembly, we measured the snRNP assembly rates in metabolically labelled wild-type and knockout cells on *UNRIP* depletion. Anti-Sm (Y12) and anti-TMG antibodies recovered equal amounts of snRNA from

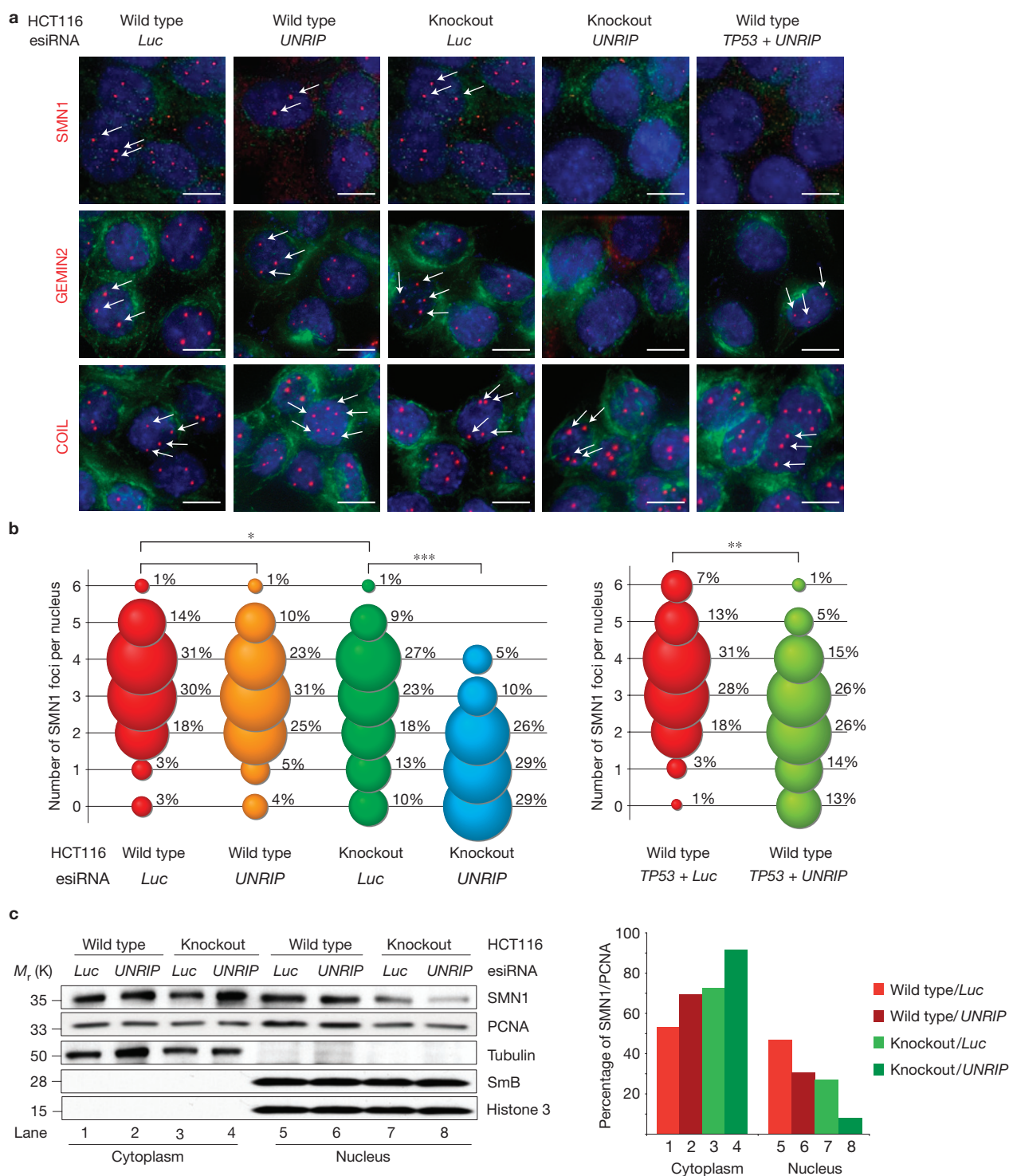


Figure 3 SMN complex localization on *UNRIP* depletion. **(a)** Immunofluorescence microscopy analysis of the cellular localization of SMN1, Gemin2 and COIL in wild-type and knockout cells on *UNRIP* depletion. Cells were stained with DAPI (4,6-diamidino-2-phenylindole; blue), α -tubulin antibody (green) and antibodies against the indicated proteins (red) for illustrated cells and knockdowns. Note that SMN1 and Gemin2 Cajal body (white arrows) localization is affected by *UNRIP* depletion only in knockout cells. Scale bars, 5 μ m. **(b)** Quantification of the number of SMN1-positive Cajal bodies per nucleus. The ball size corresponds to the percentage of cells with a particular number of foci (numerically shown on the right of each ball). The distributions of indicated cells and knockdowns were compared with Student's two-tailed

t-test, * *P* values < 0.01, ** *P* values < 10^{-5} , *** *P* values < 10^{-10} , 200–300 nuclei counted per condition in three independent experiments. Quantification of Gemin2 and COIL foci is provided in Supplementary Fig. S3a,b. **(c)** SMN1 nucleo-cytoplasmic distribution on *UNRIP* depletion. Western blot analyses of indicated proteins in cytoplasmic and nuclear extracts of control (*Luc*) and *UNRIP*-depleted wild-type and knockout cells are shown. Probing with anti-tubulin, anti-histone 3 and anti-SmB (small nuclear ribonucleoprotein polypeptides B and B1) revealed the purity of the fractions. The right panel represents quantification of SMN1 in each fraction, normalized to the amount of proliferating cell nuclear antigen (PCNA) as the loading control. Uncropped images of blots are shown in Supplementary Fig. S7b.

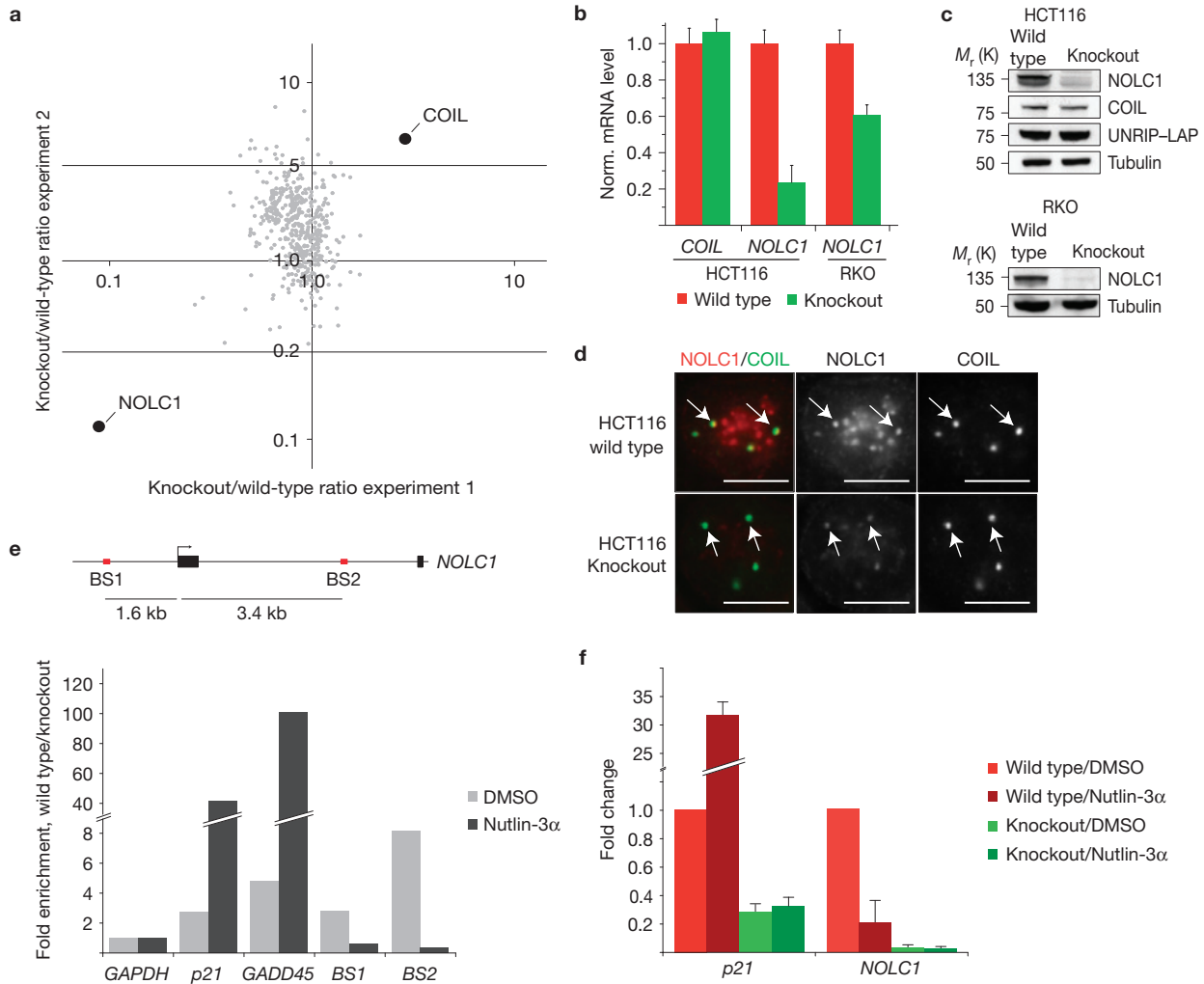


Figure 4 NOLC1 differentially associates with UNRIP in wild-type and knockout cells and *NOLC1* is a p53 target gene. **(a)** Comparative quantitative mass spectrometry of UNRIP protein complexes purified from wild-type and knockout cells. A scatter plot of the correlation of two independent pulldown experiments showing the heavy/light ratio of each identified protein purified from each cell type is illustrated. Immunoprecipitated proteins significantly over-presented (COIL) or under-presented (NOLC1) in the knockout versus the wild-type are highlighted (black dots). **(b)** Expression analysis of *COIL* and *NOLC1* mRNA. qRT-PCR results for *COIL* and *NOLC1* mRNA levels in HCT116 and RKO wild-type and knockout cells are shown. The values are normalized to the expression levels in the wild-type cells (mean \pm s.d., $n = 3$). **(c)** Western blot analysis of COIL, NOLC1 and UNRIP-LAP in HCT116 and RKO wild-type and knockout cells. **(d)** Immunofluorescence microscopy analysis

of NOLC1 (red) and COIL (green) in wild-type and knockout cells. The Cajal bodies are indicated with white arrows. Scale bars, 5 μ m. **(e)** p53 ChIP. Wild-type and knockout cells were treated with DMSO or 5 μ M Nutlin-3 α for 4 h, p53 was immunoprecipitated (DO-1 antibody) and the enrichment of selected promoter sequences was evaluated using quantitative PCR. The fold enrichment is calculated as a ratio of the percentage inputs from wild-type versus knockout samples. *GAPDH* was used to normalize this ratio. Shown is a representative experiment ($n = 3$). **(f)** *NOLC1* mRNA transcript levels are p53-dependent. HCT116 cells were treated with 5 μ M Nutlin-3 α for 4 h and the expression of *p21/WAF1* and *NOLC1* mRNA was analysed by qRT-PCR. The values are normalized to DMSO-treated wild-type cells (mean \pm s.d., $n = 3$). The response to DNA-damaging agents is presented in Supplementary Fig. S4c. Uncropped images of blots are shown in Supplementary Fig. S7c.

all samples, showing that SMN-mediated assembly and maturation of snRNPs occurs independently of UNRIP and p53 (Supplementary Fig. S3e). After snRNP core assembly and TMG cap formation, the snRNP-SMN complex is imported into the nucleus³⁷. To determine whether UNRIP plays a role in snRNP-SMN complex nuclear-cytoplasmic transport, we measured the amount of SMN1 in nuclear and cytoplasmic fractions of UNRIP-depleted cells. No prominent differences of nuclear versus cytoplasmic SMN1 were detected in control- and UNRIP-depleted wild-type cells (Fig. 3c, lane 5 and 6). In contrast, the depletion of UNRIP in knockout

cells increased cytoplasmic (Fig. 3c, lane 4 versus 3) and decreased nuclear SMN1 levels (Fig. 3c, lane 8 versus 7), indicating that UNRIP mediates SMN nuclear import or Cajal body retention with the aid of a p53-dependent factor.

NOLC1 mediates the synthetic interaction between UNRIP and TP53

In the search for a factor that mediates the SMN accumulation in Cajal bodies in a p53-dependent manner, we compared the UNRIP protein interactome in wild-type and knockout cells using

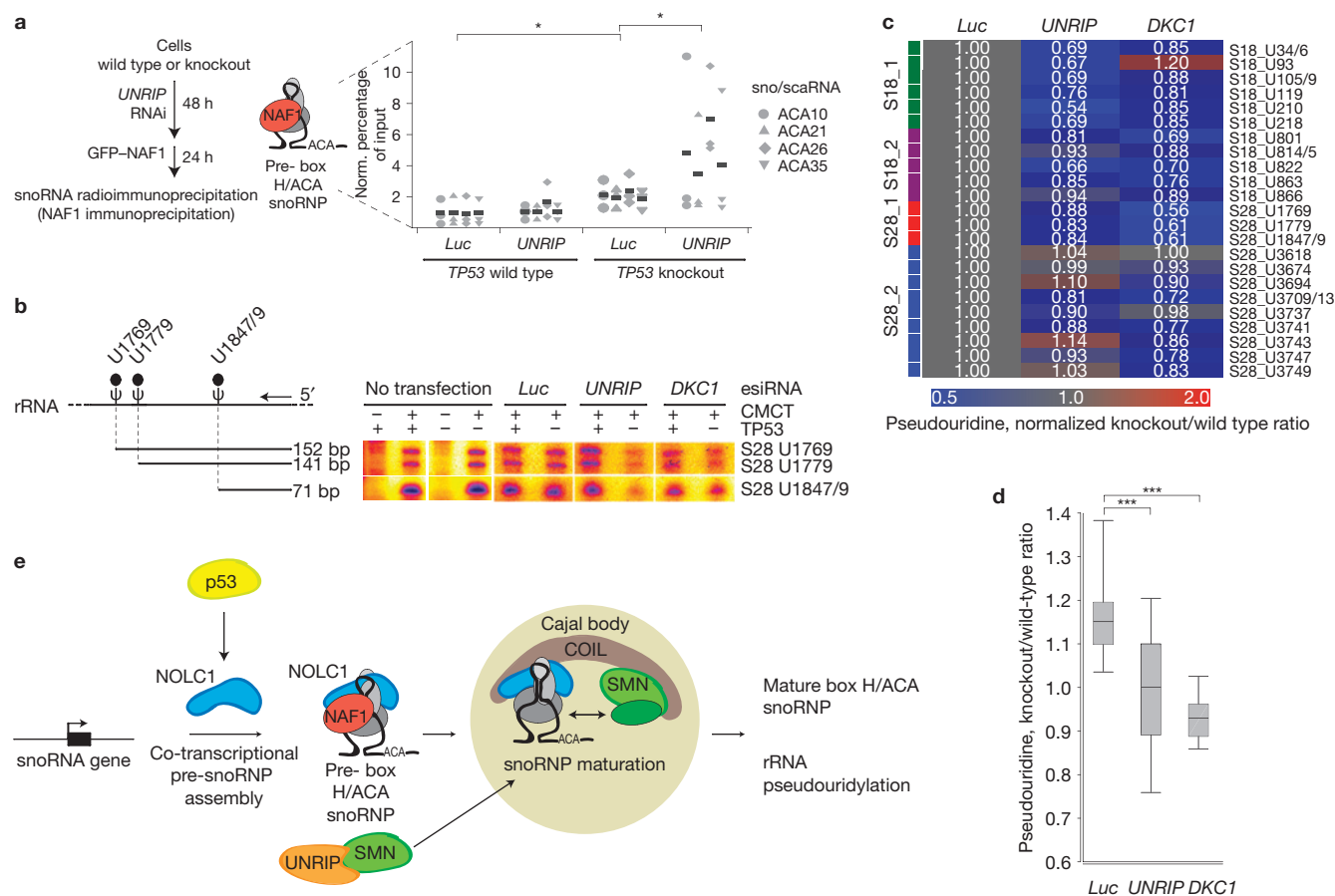


Figure 5 rRNA pseudouridylation is dependent on p53 and UNRIP. **(a)** snoRNP assembly assay. *UNRIP*-depleted HCT116 wild-type and knockout cells were transfected with a plasmid expressing GFP-NAF1. After 24 h, NAF1 was immunoprecipitated and the amount of associated pre-snoRNAs was investigated by qRT-PCR. The black bars represent mean enrichment values; significance was tested with Student's two-tailed *t*-test, * $P < 0.05$, three independent experiments. **(b)** CMCT assay for pseudouridine (ψ) detection. After CMCT modification of total cellular RNA, primers were hybridized to targeted regions of the rRNA and reverse-transcriptase reactions determined the modified pseudouridine sites (black ball). Equal amounts of RNA were loaded in all reactions. The greyscale intensities are colour-coded for indicated treatments. **(c, d)** Quantification of the amount of pseudouridylation at 24 sites in 18S and 28S rRNA on a per site **(c)** or per treatment **(d)** basis. The colour-coding represents the knockout/wild-type ratio (blue, decreased;

red, increased) of the intensities of the pseudouridine sites for indicated treatments, with the ratio of the *Luc* control for each site set to 1. The sites are clustered according to the primer with which they were detected (18S_1, green; 18S_2, purple; 28S_1, red; 28S_2, blue). The box plot shows the averaged values of knockout/wild-type pseudouridine ratios of the 24 tested sites for the indicated treatments. The whiskers denote the 10th and 90th percentiles of the values, respectively. The significance was tested with Student's paired two-tailed *t*-test, *** $P < 0.001$, $n = 24$, three independent experiments. **(e)** Model summarizing the synthetic interaction between *TP53* and *UNRIP*. *UNRIP* is required to bring the SMN complex into the Cajal bodies. *TP53* regulates the levels of *NOLC1*, which brings the immature snoRNPs into the Cajal bodies, where on interaction with *COIL* and *SMN* the mature snoRNPs are assembled. Thus, absence of *TP53* synergizes with decreased *UNRIP* levels to perturb snoRNP assembly and in turn this decreases the level of pseudouridylation of rRNA.

quantitative BAC (bacterial artificial chromosome) interactomics³⁸ (QUBIC). Wild-type and knockout cells expressing LAP-tagged *UNRIP* were SILAC (stable isotope labelling of amino acids in cell culture)-labelled with either light (¹²C¹⁴N) or heavy (¹³C¹⁵N) isotopes in cell culture, respectively³⁹. Anti-GFP pull-downs of 'light' wild-type and 'heavy' knockout cells were carried out. Each peptide was therefore present in a 'light' and 'heavy' form, representing relative protein abundance in wild-type and *TP53*-knockout cells. Most proteins had a heavy/light ratio of 1:1, as they either show no differential binding in knockout versus wild-type cells or represent background binding to the affinity matrix. For example, *UNRIP*-LAP interacted with the SMN complex, as well as with other Cajal body proteins, with equal affinity in both cell lines (Fig. 4a and Table 2). Strikingly, two proteins showed significantly different ratios—*COIL* (ratio of

about 4) was enriched and nucleolar protein *NOLC1* (nucleolar and coiled-body phosphoprotein 1; ratio of about 0.1) was under-presented in pull-downs from the knockout when compared with wild-type cells. Quantitative PCR with reverse transcription (qRT-PCR), western blot and immunofluorescence microscopy analyses showed that *NOLC1*, but not *COIL*, mRNA and protein levels are generally lower in knockout cells in comparison with wild-type cells (Fig. 4b–d), indicating that *NOLC1* is a p53-regulated gene. Importantly, the same reduced *NOLC1* levels were also observed in *TP53*-knockout RKO cells, indicating that this effect is not specific to HCT116 cells (Fig. 4b,c). p53scan software⁴⁰ predicted four putative p53-binding sites within the *NOLC1* genomic sequence (Supplementary Fig. S4a,b). Carrying out p53 chromatin immunoprecipitation (ChIP) experiments, we identified significant enrichment for two sites, one located 1.6 kb upstream

Table 2 Comparative UNRIP proteomics.

Protein	IPI	Seq. cov. (%)	'Heavy' knockout versus 'light' wild type		'Heavy' wild type versus 'light' knockout (reciprocal values)	
			Unique peptides	SILAC ratio	Unique peptides	SILAC ratio
UNRIP	IPI00294536	97	29	1.000	33	1.000
UNR	IPI00470891	69	46	1.280	52	0.802
SMN1	IPI00003394	34	11	1.094	9	1.241
GEMIN2	IPI00024281	72	14	0.985	12	1.618
GEMIN3	IPI00005904	58	35	1.214	35	1.241
GEMIN4	IPI00027717	47	39	1.163	38	1.512
GEMIN5	IPI00291783	38	14	0.977	16	1.000
GEMIN6	IPI00103087	55	8	1.203	8	1.812
GEMIN7	IPI00003027	84	6	1.185	4	1.376
GEMIN8	IPI00301879	39	4	1.130	7	1.773
SNRPB	IPI00329512	39	4	1.144	6	1.736
SNRPC	IPI00641788	39	1	NA	2	1.618
SNRPD1	IPI00903286	44	4	1.060	3	1.736
SNRPD2	IPI00017963	59	10	1.115	10	1.232
SNRPD3	IPI00879750	38	4	1.080	5	1.486
SNRPE	IPI00029266	70	3	0.989	4	1.792
SNRPF	IPI00220528	58	5	1.055	6	2.141
SNRPG	IPI00745343	37	2	1.121	4	1.603
SNRP70	IPI00290204	75	7	1.026	6	1.205
NOLC1	IPI00216654	30	12	0.086	8	0.116
COIL	IPI00006442	12	3	2.959	4	4.854
C1ORF144	IPI00470594	52	7	0.931	6	1.309

IPI, International Protein Index; Seq. cov., sequence coverage; NA, not available.

(BS1) and another located 3.4 kb downstream (BS2) of the *NOLC1* transcription initiation start site, respectively (Fig. 4e). Typically, on stress activation, p53 binds to its response elements in target genes and leads to their upregulation or downregulation. Surprisingly, p53 ChIP signals at *NOLC1* BS1 and BS2 decreased markedly on p53 induction (Fig. 4e), indicating that p53 leaves these sites under stress conditions. Furthermore, *NOLC1* mRNA levels decreased fourfold in p53-stimulated wild-type cells (Fig. 4f and Supplementary Fig. S4c). Consistent with the idea that p53 vacates the promoter under stress conditions, we observed downregulation of reporter constructs harbouring the BS1 sequence on p53 overexpression (Supplementary Fig. S4d). Collectively, these experiments identify *NOLC1* as a p53 target gene whose continuous expression is dependent on physiological levels of p53. To our knowledge, this is the first report of a p53 target gene that is downregulated not by p53 recruitment and active repression, but rather by p53 promoter vacation.

snoRNP functions are affected in a p53- and UNRIP-dependent manner

NOLC1 is a nuclear phosphoprotein that has previously been localized to Cajal bodies and nucleoli^{41,42}. Cajal body localization is mediated by direct interactions with COIL and is SMN-dependent^{43,44}. As both NOLC1 and SMN interact with core snoRNP components, they may have a role in snoRNP assembly in Cajal bodies^{45–47}. NOLC1 has also been suggested to participate in snoRNP trafficking⁴⁸ and stability⁴⁶. We investigated whether any of these functions is the basis for the observed knockout-specific phenotype. The steady-state levels of the mature snoRNAs were not affected by either *NOLC1* or *UNRIP* depletion (Supplementary Fig. S5a). Furthermore, RNA fluorescent *in situ* hybridization revealed that the cellular localization of five examined snoRNAs was not altered under the same conditions (Supplementary Fig. S5b). Next, we examined possible defects in the assembly of *de novo* synthesized snoRNPs. To assess the rate of snoRNP assembly, we first measured the association of newly synthesized snoRNAs

with NAF1 (nuclear assembly factor 1 homologue), a protein that binds the immature snoRNPs (ref. 49). We transfected control- (*Luc*) and *UNRIP*-depleted wild-type or knockout cells with a plasmid expressing GFP-NAF1, followed by NAF1 immunoprecipitation and quantification of associated snoRNAs. Control-depleted knockout cells showed about twofold enrichment of snoRNAs in comparison with control-depleted wild-type cells, indicating a delay in snoRNA maturation, possibly due to the decreased NOLC1 levels (Fig. 5a). This enrichment was further enhanced specifically in *UNRIP*-depleted knockout cells, indicating that both *NOLC1* and *UNRIP* are needed for efficient snoRNP assembly. Finally, we assessed snoRNA assembly by measuring the amounts of snoRNP-catalysed modifications in the rRNA. Pulse-chase metabolic labelling experiments revealed that rRNA cleavage patterns and rRNA methylation (catalysed by the box C/D snoRNPs) were unaffected in cells of all investigated conditions (Supplementary Fig. S6a–c). Last, we measured the amounts of pseudouridines in functionally important regions of the rRNA (ref. 50), the formation of which is catalysed by the box H/ACA snoRNPs. Figure 5b–d shows the quantified ratio of pseudouridine (knockout/wild-type signal) in *UNRIP*- and control-depleted cells for 24 sites of 18S and 28S rRNAs. Remarkably, *UNRIP* depletion led to decreased levels of pseudouridylation at most of the 24 sites assayed; the effects of *UNRIP* depletion were often as strong or stronger than the depletion of the enzyme dyskerin (*DKC1*), which catalyses the reaction⁵¹. This survey of 24 out of about 100 pseudouridylation sites on rRNA establishes the generality of the effects seen here. The fact that both *UNRIP* and *DKC1* depletion led to decreased levels of pseudouridylation preferentially in the knockout cells, together with the increased association of pre-snoRNAs with NAF1, indicates that snoRNP assembly and subsequent function is the underlying vulnerability in these cells. Collectively, these experiments demonstrate that NOLC1 and UNRIP (through SMN) act synergistically in the Cajal body to assemble snoRNPs and provide the molecular explanation for the synthetic interaction between *UNRIP* and *TP53*.

DISCUSSION

Our data are consistent with a model in which snoRNP assembly in the Cajal body is the process in which *TP53* and *UNRIP* genetically interact (Fig. 5e). p53 regulates *NOLC1* steady-state levels and *UNRIP* contributes to nuclear SMN import. *NOLC1* and SMN support snoRNP assembly in the Cajal bodies and their localization there is mutually dependent. This effect seems to be preferentially important for the box H/ACA snoRNPs. Thus, decreased *NOLC1* levels in the knockout cells sensitizes them to the amount of nuclear SMN, which explains their increased dependency on *UNRIP* for efficient growth and proliferation. This model is substantiated by findings in other model organisms. *NOLC1* preferentially affects the box H/ACA snoRNPs^{46,52}, and the gradual loss of pseudouridines in rRNA correlates with decreased proliferation⁵⁰. Furthermore, in *Drosophila*, depletion of *NOLC1* expression levels by RNAi leads to development of a *Minute* phenotype⁵³ and in humans the loss of *TCOF1*, the paralogue of *NOLC1*, leads to development of Treacher–Collins syndrome⁵⁴, both conditions caused by a loss of ribosome functions. All of these observations show that the rate of cellular proliferation can be adjusted by the rate of ribosome biogenesis.

Our finding that continuous expression of *NOLC1* under normal growth conditions is attuned by p53 implies that p53 exerts its influence over the ribosome biogenesis pathway; it adjusts the cellular growth and acts in a positive feedback loop of the RP–Hdm2–p53 pathway²⁶ to limit ribosome assembly and cellular proliferation under stress conditions. In accordance, p53 upregulation leads to *NOLC1* downregulation. Interestingly, this repression seems to be mediated through vacation of p53 from its binding sites in the *NOLC1* promoter, possibly due to competition with other transcription factors or large intergenic non-coding RNA (ref. 55). This so far uncharacterized homeostatic function of p53 provides yet another mechanism for synchronization of the optimal cellular growth with the environment, which is sensed by p53. As a consequence, p53–negative cells become unable to maintain appropriate growth rates and become vulnerable to interference with specific other processes, such as snoRNP assembly. □

METHODS

Methods and any associated references are available in the online version of the paper at <http://www.nature.com/naturecellbiology>

Note: Supplementary Information is available on the Nature Cell Biology website

ACKNOWLEDGEMENTS

We would like to thank all members of the Buchholz laboratory for discussions and sharing reagents. We thank A. K. Heninger for help with carrying out the screen, V. Surendranath for esiRNA design, M. Theis, S. Rose and A. Weise for esiRNA production and I. Poser for assistance with BAC cell line generation. This work was supported by the Max Planck Society, the German Federal Ministry of Education and Research grants Go-Bio (0315105), DiGtoP (01GS0859) and the DFG grant SFB655.

AUTHOR CONTRIBUTIONS

D.B.K., M.S., N.C.H., M.J. and K.M.N. carried out experiments, M.P.-R. analysed data, A.S., M.M. and F.B. planned the project and D.B.K. and F.B. wrote the manuscript.

COMPETING FINANCIAL INTERESTS

The authors declare no competing financial interests.

Published online at <http://www.nature.com/naturecellbiology>

Reprints and permissions information is available online at <http://www.nature.com/reprints>

- Levine, A. J. & Oren, M. The first 30 years of p53: growing ever more complex. *Nat. Rev. Cancer* **9**, 749–758 (2009).
- Toledo, F. & Wahl, G. M. Regulating the p53 pathway: *in vitro* hypotheses, *in vivo* veritas. *Nat. Rev. Cancer* **6**, 909–923 (2006).
- Riley, T., Sontag, E., Chen, P. & Levine, A. Transcriptional control of human p53-regulated genes. *Nat. Rev. Mol. Cell Biol.* **9**, 402–412 (2008).
- Olovnikov, I. A., Kravchenko, J. E. & Chumakov, P. M. Homeostatic functions of the p53 tumor suppressor: regulation of energy metabolism and antioxidant defense. *Semin. Cancer Biol.* **19**, 32–41 (2009).
- Matoba, S. *et al.* p53 regulates mitochondrial respiration. *Science* **312**, 1650–1653 (2006).
- Sablina, A. A. *et al.* The antioxidant function of the p53 tumor suppressor. *Nature Med.* **11**, 1306–1313 (2005).
- Bensaad, K. *et al.* TIGAR, a p53-inducible regulator of glycolysis and apoptosis. *Cell* **126**, 107–120 (2006).
- Kawamura, T. *et al.* Linking the p53 tumour suppressor pathway to somatic cell reprogramming. *Nature* **460**, 1140–1144 (2009).
- Hu, W., Feng, Z., Teresky, A. K. & Levine, A. J. p53 regulates maternal reproduction through LIF. *Nature* **450**, 721–724 (2007).
- Beltrao, P., Cagney, G. & Krogan, N. J. Quantitative genetic interactions reveal biological modularity. *Cell* **141**, 739–745 (2010).
- Kaelin, W. G. The concept of synthetic lethality in the context of anticancer therapy. *Nat. Rev. Cancer* **5**, 689–698 (2005).
- Luo, J. *et al.* A genome-wide RNAi screen identifies multiple synthetic lethal interactions with the ras oncogene. *Cell* **137**, 835–848 (2009).
- Scholl, C. *et al.* Synthetic lethal interaction between oncogenic KRAS dependency and STK33 suppression in human cancer cells. *Cell* **137**, 821–834 (2009).
- MacKeigan, J. P., Murphy, L. O. & Blenis, J. Sensitized RNAi screen of human kinases and phosphatases identifies new regulators of apoptosis and chemoresistance. *Nat. Cell Biol.* **7**, 591–600 (2005).
- Whitehurst, A. W. *et al.* Synthetic lethal screen identification of chemosensitizer loci in cancer cells. *Nature* **446**, 815–819 (2007).
- Bommi-Reddy, A. *et al.* Kinase requirements in human cells: III. Altered kinase requirements in VHL–/– cancer cells detected in a pilot synthetic lethal screen. *Proc. Natl Acad. Sci. USA* **105**, 16484–16489 (2008).
- Bunz, F. *et al.* Requirement for p53 and p21 to sustain G2 arrest after DNA damage. *Science* **282**, 1497–1501 (1998).
- Vassilev, L. T. *et al.* *In vivo* activation of the p53 pathway by small-molecule antagonists of MDM2. *Science* **303**, 844–848 (2004).
- Shvarts, A. *et al.* MDMX: a novel p53-binding protein with some functional properties of MDM2. *EMBO J.* **15**, 5349–5357 (1996).
- Kittler, R. *et al.* Genome-scale RNAi profiling of cell division in human tissue culture cells. *Nat. Cell Biol.* **9**, 1401–1412 (2007).
- Theis, M. *et al.* Comparative profiling identifies C13orf3 as a component of the Ska complex required for mammalian cell division. *EMBO J.* **28**, 1453–1465 (2009).
- Slabicki, M. *et al.* A genome-scale DNA repair RNAi screen identifies SPG48 as a novel gene associated with hereditary spastic paraplegia. *PLoS Biol.* **8**, e1000408 (2010).
- Matthews, L. *et al.* Reactome knowledgebase of human biological pathways and processes. *Nucl. Acids Res.* **37**, D619–D622 (2009).
- Jensen, L. *et al.* STRING 8—a global view on proteins and their functional interactions in 630 organisms. *Nucl. Acids Res.* **37**, D412–D416 (2009).
- Zhang, X. D. *et al.* Robust statistical methods for hit selection in RNAi interference high-throughput screening experiments. *Pharmacogenomics* **7**, 299–309 (2006).
- Deisenroth, C. & Zhang, Y. Ribosome biogenesis surveillance: probing the ribosomal protein-Mdm2-p53 pathway. *Oncogene* **29**, 1–8 (2010).
- Fromont-Racine, M., Senger, B., Saveanu, C. & Fasiolo, F. Ribosome assembly in eukaryotes. *Gene* **313**, 17–42 (2003).
- Sur, S. *et al.* A panel of isogenic human cancer cells suggests a therapeutic approach for cancers with inactivated p53. *Proc. Natl Acad. Sci. USA* **106**, 3964–3969 (2009).
- Datta, P. K., Chytil, A., Gorska, A. E. & Moses, H. L. Identification of STRAP, a novel WD domain protein in transforming growth factor- β signaling. *J. Biol. Chem.* **273**, 34671–34674 (1998).
- Carissimi, C. *et al.* Unrip is a component of SMN complexes active in snRNP assembly. *FEBS Lett.* **579**, 2348–2354 (2005).
- Kittler, R. *et al.* RNA interference rescue by bacterial artificial chromosome transgenesis in mammalian tissue culture cells. *Proc. Natl Acad. Sci. USA* **102**, 2396–2401 (2005).
- Poser, I. *et al.* BAC TransgeneOmics: a high-throughput method for exploration of protein function in mammals. *Nat. Methods* **5**, 409–415 (2008).
- Battle, D. *et al.* The SMN complex: an assembly machine for RNPs. *Cold Spring Harb. Symp. Quant. Biol.* **71**, 313–320 (2006).
- Hao, L. T. *et al.* Absence of gemin5 from SMN complexes in nuclear Cajal bodies. *BMC Cell Biol.* **8**, 28 (2007).
- Narayanan, U., Achsel, T., Lührmann, R. & Matera, A. G. Coupled *in vitro* import of U snRNPs and SMN, the spinal muscular atrophy protein. *Mol. Cell* **16**, 223–234 (2004).

36. Fischer, U., Sumpter, V., Sekine, M., Satoh, T. & Luhrmann, R. Nucleo-cytoplasmic transport of U snRNPs: definition of a nuclear location signal in the Sm core domain that binds a transport receptor independently of the m3G cap. *EMBO J.* **12**, 573–583 (1993).
37. Hamm, J., Darzynkiewicz, E., Tahara, S. M. & Mattaj, I. W. The trimethylguanosine cap structure of U1 snRNA is a component of a bipartite nuclear targeting signal. *Cell* **62**, 569–577 (1990).
38. Hubner, N. C. *et al.* Quantitative proteomics combined with BAC TransGeneOmics reveals *in vivo* protein interactions. *J. Cell Biol.* **189**, 739–754 (2010).
39. Ong, S. E. *et al.* Stable isotope labelling by amino acids in cell culture, SILAC, as a simple and accurate approach to expression proteomics. *Mol. Cell Proteomics* **1**, 376–386 (2002).
40. Smeenk, L. *et al.* Characterization of genome-wide p53-binding sites on stress response. *Nucleic Acids Res.* **17**, 3639–3654 (2008).
41. Meier, U. T. & Blobel, G. Nopp140 shuttles on tracks between nucleolus and cytoplasm. *Cell* **70**, 127–138 (1992).
42. Pai, C. Y., Chen, H. K., Sheu, H. L. & Yeh, N. H. Cell-cycle-dependent alterations of a highly phosphorylated nucleolar protein p130 are associated with nucleologenesis. *J. Cell Sci.* **108**, 1911–1920 (1995).
43. Isaac, C., Yang, Y. & Meier, U. T. Nopp140 functions as a molecular link between the nucleolus and the coiled bodies. *J. Cell Biol.* **142**, 319–329 (1998).
44. Renvoise, B. *et al.* The loss of the snoRNP chaperone Nopp140 from Cajal bodies of patient fibroblasts correlates with the severity of spinal muscular atrophy. *Hum. Mol. Genet.* **18**, 1181–1189 (2009).
45. Pellizzoni, L., Baccon, J., Charroux, B. & Dreyfuss, G. The survival of motor neurons (SMN) protein interacts with the snoRNP proteins fibrillarin and GAR1. *Curr. Biol.* **11**, 1079–1088 (2001).
46. Yang, Y. *et al.* Conserved composition of mammalian box H/ACA and box C/D small nucleolar ribonucleoprotein particles and their interaction with the common factor Nopp140. *Mol. Biol. Cell* **11**, 567–577 (2000).
47. Wang, C., Query, C. C. & Meier, U. T. Immunopurified small nucleolar ribonucleoprotein particles pseudouridylylate rRNA independently of their association with phosphorylated Nopp140. *Mol. Cell Biol.* **22**, 8457–8466 (2002).
48. Verheggen, C. *et al.* Box C/D small nucleolar RNA trafficking involves small nucleolar RNP proteins, nucleolar factors and a novel nuclear domain. *EMBO J.* **20**, 5480–5490 (2001).
49. Darzacq, X. *et al.* Stepwise RNP assembly at the site of H/ACA RNA transcription in human cells. *J. Cell Biol.* **173**, 207–218 (2006).
50. King, T. H., Liu, B., McCully, R. R. & Fournier, M. J. Ribosome structure and activity are altered in cells lacking snoRNPs that form pseudouridines in the peptidyl transferase center. *Mol. Cell* **11**, 425–435 (2003).
51. Lafontaine, D. L., Bousquet-Antonelli, C., Henry, Y., Caizergues-Ferrer, M. & Tollervey, D. The box H+ACA snoRNAs carry Cbf5p, the putative rRNA pseudouridine synthase. *Genes Dev.* **12**, 527–537 (1998).
52. Yang, Y. & Meier, U. T. Genetic interaction between a chaperone of small nucleolar ribonucleoprotein particles and cytosolic serine hydroxymethyltransferase. *J. Biol. Chem.* **278**, 23553–23560 (2003).
53. Cui, Z. & DiMario, P. J. RNAi knockdown of Nopp140 induces Minute-like phenotypes in *Drosophila*. *Mol. Biol. Cell* **18**, 2179–2191 (2007).
54. Isaac, C. *et al.* Characterization of the nucleolar gene product, treacle, in Treacher Collins syndrome. *Mol. Biol. Cell* **11**, 3061–3071 (2000).
55. Huarte, M. *et al.* A large intergenic noncoding RNA induced by p53 mediates global gene repression in the p53 response. *Cell* **143**, 409–419 (2010).

METHODS

Cell culture, constructs and reagents. HCT116 and RKO (wild-type and *TP53* knockout) cells (kind gift from B. Vogelstein, Sidney Kimmel Comprehensive Cancer Center, Johns Hopkins University, Baltimore, USA) were maintained in 4.5 mg ml⁻¹ glucose DMEM, supplemented with 10% FBS (Invitrogen), 100 U ml⁻¹ penicillin and 100 µg ml⁻¹ streptomycin (Gibco-Invitrogen). Enhanced GFP (EGFP)-tagged nuclear localization signal (NLS) protein and mRed-NLS were cloned into pIRESpuro3 plasmid (Clontech) and stable cell lines were selected with 1 µg ml⁻¹ puromycin (Sigma-Aldrich). BAC clones RP11-413P14 and RP24-191F17 encoding human and mouse *UNRIP* genes respectively were obtained from BACPAC resource. They were tagged as previously described³² and stable cell lines were selected on the basis of their neomycin (0.5 mg ml⁻¹, Invitrogen) or blasticidin (5 µg ml⁻¹, Invitrogen) resistance.

The following antibodies and proteins were used: anti-GFP (Roche, MPI-CBG, 1:5,000), anti- α -tubulin (MPI-CBG, 1:50,000), anti-UNRIP (sc-14552, 1:1,000), anti-SMN1 (ab5831, 1:1,000), anti-Gemin2 (ab6084, 1:1,000), anti-SmB (sc-25372, 1:1,000), anti-COIL (1:500; ref. 56; sc-32860, 1:500), anti-PCNA (sc-9857, 1:1,000), anti-p53 (DO-1), anti-NOLC1 (sc-101101, 1:1,000), anti-histone3 (ab1791, 1:10,000), anti-p21/WAF1 (sc-6246, 1:1,000), camptothecin (Sigma-Aldrich), bleocin (Merck Bioscience) and Nutlin-3 α (Sigma-Aldrich). p21-luc (ref. 57), 3TP-luc (ref. 58), pCS2-Smad2 (ref. 59) and pRK5-T202D (ref. 60) were obtained from the Addgene repository and the Smad reporter kit was from SuperArray. The GFP-NAF1-expressing plasmid was a kind gift from U. T. Meier⁴⁹ (Department of Anatomy and Structural Biology, Albert Einstein College of Medicine, New York, USA). The *NOLC1* promoter sequence was amplified and cloned into pGL4.10 (Promega) reporter plasmid. *UNRIP* Mission shRNA-expressing plasmids (shRNA1—NM_007178.2-981s1c1 and shRNA—NM_007178.2-981s1c1) were from Sigma-Aldrich.

esiRNA preparation and library construction were carried out as previously described⁶¹. Typically, HCT116 cells were transfected in 384-well plates with 25 ng esiRNA and 0.25 µl Oligofectamine (Invitrogen) in 10 µl OptiMem (Invitrogen). For transfections in other plate formats the esiRNA amounts were scaled according to the surface area of the wells.

High-throughput screen, data analysis and hits validation. A total of 1,000 wild-type and 1,000 knockout HCT116 cells, in 100 µl of cell suspension, were reverse transfected in black 384-well tissue culture plates (Greiner). Plates were sealed with breathable foil (Corning) and incubated for 96 h. Cells were fixed and four images per well were acquired using a ScanR screening station (Olympus). The number of wild-type and knockout cells was exported with the ScanR analysis software. The screen was conducted in two replicates. Each plate contained twelve negative (luciferase) and four positive (*HDMX*) control esiRNAs. The cell numbers (Supplementary Table S1) for each esiRNA knockdown (each well position) were calculated for the wild-type and knockout cells separately:

$$X_{i,p} = \frac{X_{i,p}(\text{raw})}{\bar{X}} \times \bar{X}_p$$

$X_{i,p}$ is the cell number of well i and plate p , $X_{i,p}(\text{raw})$ is the cell number extracted from the image analysis, \bar{X} is the cell number of well i averaged over all plates and \bar{X}_p is the average cell number of all wells in plate p . The $X_{i,p}$ values were used to calculate the wild-type/knockout ratio. The z scores of the cell numbers, showing how many standard deviations (σ_p) the observed cell number ($X_{i,p}$) is different from the mean cell number (\bar{X}_p), is calculated in a plate-wise manner.

$$z = \frac{X_{i,p} - \bar{X}_p}{\sigma_p}$$

A viability phenotype was assigned to each esiRNA with z scores for both wild-type and knockout cells lower than -2 (or -1.5) in any of the technical replicates of the screen. Using a quartile-based threshold we divide the $\log_2(\text{wild-type/knockout})$ into three phenotypic categories in a plate-wise manner:

Decreased wild-type/knockout ratio	-1	$X_i < Q_1 - 2c(Q_2 - Q_1)$
No change in wild-type/knockout ratio	0	$X_i \in (Q_1 - 2c(Q_2 - Q_1); Q_3 + 2c(Q_3 - Q_2))$
Increased wild-type/knockout ratio	1	$X_i > Q_3 + 2c(Q_3 - Q_2)$

where X_i denotes the $\log_2(\text{wild-type/knockout})$ for a given esiRNA, Q_1 , Q_2 and Q_3 are the first, second and third quartile values of the corresponding plate and c is a constant, which can be chosen depending on the targeted error rate under the null hypothesis (for an error rate of 0.05 $c = 0.9529$; ref. 25). The primary hits were selected on the basis of the condition of scoring as 1 or -1 in both technical replicates. For the validation screens and secondary esiRNAs, z scores (always of wild-type/knockout ratio) are calculated on the basis of the variation of

negative control transfections (luciferase). From each set of controls and treatment samples up to one outlier was removed on the basis of Grubb's outlier removal test. Phenotypes were considered validated when they were statistically significant according to Student's t -test ($P < 0.05$).

Time-lapse analysis. HCT116 wild-type and knockout cells were mixed in a 1:1 ratio and reverse transfected with esiRNAs. At 24 h post-transfection, the cells were imaged for another 72 h with an image acquired every 30 min with a Scan R imaging system (Olympus). Doubling times were calculated from exponential fits to the growth curves.

Colony formation assay. RNAi-treated cells were trypsinized 24 h post-transfection; 2,000 cells were seeded in six-well plates and cultivated for a week. Colonies were fixed with paraformaldehyde and stained with 0.05% crystal violet (Sigma). The number of colonies was analysed with Cell Profiler software⁶² or absorbance at 540 nm was determined after methanol extraction.

Luciferase assay. All firefly constructs were mixed in a 40:1 ratio with a constitutive Renilla-expressing luciferase construct, pGL4.73 (Promega). The co-transfection of esiRNA and plasmid DNA was carried out with SureFECT transfection reagent (SuperArray). Luciferase luminescence was measured with the Dual-Glo Luciferase Assay System (Promega) on a GENios pro plate reader (Tecan). The firefly signal was normalized to the Renilla signal and the average and standard deviation of at least three independent experiments are presented.

Immunoprecipitation, mass-spectrometry and QUBIC experiments. Immunoprecipitation reactions were carried out with extracts from cells expressing LAP-tagged proteins and subjected to shotgun mass spectrometry (MS) as previously described^{21,32}. Briefly, LAP-tagged proteins were immunoprecipitated with anti-GFP antibody (MPI-CBG) coupled to G-protein Sepharose (GE Healthcare). Glycine-eluted complexes were digested in solution using trypsin, and the resulting peptides were analysed by shotgun liquid chromatography-MS/MS on an LTQ Orbitrap (Thermo Fisher Scientific)⁶³. Proteins identified in more than 15% of more than 200 immunoprecipitations from unrelated bait proteins were considered as common background proteins and were excluded from further analysis. For QUBIC, HCT116 wild-type or knockout cells expressing human UNRIP-LAP were SILAC-labelled⁶⁴ in DMEM media, supplemented with heavy- (¹³C¹⁵N) or light- (¹²C¹⁴N) isotope-labelled arginine and lysine. After seven days, extracts were prepared from 2×10^7 cells and complexes were precipitated with an anti-GFP antibody (Miltenyi Biotec). The eluted proteins were mixed in a 1:1 ratio and subjected to mass spectrometry³⁸. The experiment was repeated with extracts from reverse labelled cells.

qRT-PCR. At 48 h post-transfection, total RNA was isolated with an RNeasy Mini Kit (Qiagen) and 500 ng was reverse transcribed with SuperScript III reverse transcriptase (Invitrogen). Quantitative PCR reactions were carried out with the SYBR Green qPCR kit (Abgene) on an MX P3000 qPCR machine (Stratagene) according to the manufacturer's recommendations. Relative mRNA levels were calculated according to the $\Delta\Delta C_t$ threshold cycle method and normalized to the luciferase control; GAPDH was used as an internal loading control.

Immunofluorescence microscopy. Cells were seeded on coverslips in 24-well plates, transfected 24 h later and immunostained as previously described²¹. Images were acquired on an Axioplan II microscope (Zeiss) operated by MetaMorph (Molecular Devices) or on an Olympus IX70 microscope (Olympus) equipped with a DeltaVision RT imaging system. For nuclear foci scoring, z stacks were acquired, deconvolved and projected into a single plane using softWoRx software. Contrast levels were manually adjusted and at least 200–300 cell nuclei were manually scored per sample. The distributions were compared using Student's two-tailed t -test.

Cell fractionation. Cell fractionation experiments were carried out with the ProteoExtract Subcellular Proteome Extraction Kit (Calbiochem) according to the manufacturer's recommendations.

p53 ChIP. HCT116 cells (2×10^7) were treated with 5 µM Nutlin-3 α for 4 h and p53 was precipitated with 4 µg DO-1 antibody as described previously⁶⁵. The fold change was calculated as the ratio of the percentage inputs from wild-type and knockout cells.

snRNP assembly assay. The snRNP immunoprecipitation protocol was modified from ref. 56. Briefly, at 36 h post-transfection the medium was replaced with phosphate-free DMEM medium (Gibco, Invitrogen) supplemented with 20 µCi ml⁻¹ ³²P-orthophosphate. After 16 h incubation, the cells were scraped into NET-2 buffer (50 mM Tris-HCl at pH 7.5, 150 mM NaCl and 0.05% NP-40), sonicated and centrifuged to remove debris and unlysed cells. The cell extract

was incubated with Y12- (recognizes the Sm ring⁶⁶) or anti-TMG- (recognizes the tri-methylated cap; NA02 Merk Bioscience) conjugated Gammabind G beads (GE Healthcare). Bound RNA was extracted with phenol/chloroform and precipitated overnight with ethanol. The RNA samples were resolved on a denaturing 7 M urea 10% PAGE gel and imaged with a phosphoimager (Fujifilm BAS-1800II).

snRNP assembly assay. Cells were seeded in six-well plates and subjected to RNAi for 48 h, followed by overexpression of GFP–NAF1 for a further 24 h. A quantity of 100 µg total cellular extract (prepared in NET-2 buffer) was incubated with 50 µl GFP–Trap beads (ChromoTek) and associated pre-snoRNAs were phenol-purified, DNase-I-treated and reverse transcribed with specific pre-snoRNA primers.

Metabolic labelling and pulse-chase assays. rRNA cleavage maturation was investigated in ³²P-orthophosphate labelled cells. Briefly, before labelling, the cells were incubated in P-free DMEM media (Invitrogen) for 1 h, labelled with 20 µCi ml⁻¹ ³²P-orthophosphate for 1 h and chased with normal growth media for 30 min. Total RNA was extracted with Trizol (Invitrogen), and 5 µg was resolved on a denaturing agarose gel and autoradiographed for 24 h. For rRNA methylation, the cells were incubated in methionine-free MEM media (Invitrogen) for 15 min before being labelled with 50 µCi ml⁻¹ L-[methyl-³H]-methionine for 30 min and chased with 0.3 mg ml⁻¹ methionine-containing DMEM for 30 min. Total RNA was extracted with Trizol (Invitrogen), and 5 µg was resolved on a denaturing agarose gel, transferred to a nitrocellulose membrane and autoradiographed for 3–5 days.

RNA fluorescence *in situ* hybridization. The mature snoRNAs were amplified from a total RNA sample and the PCR products were used as a template for *in vitro* RNA transcription with SP6 polymerase (MPI–CBG) in the presence of FITC (fluorescein isothiocyanate)-conjugated UTP (Invitrogen). The hybridization was conducted as described previously⁶⁷.

CMCT assay. CMCT (*N*-cyclohexyl-*N'*-β-(4-methylmorpholinium)ethylcarboxy diimide p-tosylate) modification of RNA was carried out as described previously⁶⁸. Briefly, total RNA from RNAi-depleted HCT116 cells was extracted with Trizol (Invitrogen) and 10 µg was CMCT modified. A quantity of 0.5 µg modified RNA was used in primer extension reactions with SuperScript III reverse transcriptase (Invitrogen) and the primers 28S_1, 28S_2, 18S_1 and 18S_2. The products were resolved on denaturing 10% PAGE and quantified on a phosphoimager (Fujifilm

BAS-1800II). Equal loading of the lanes was ensured by northern blot analysis of the 28S rRNA.

All primers used in this study are listed in Supplementary Table S4.

56. Pettersson, I., Hinterberger, M., Mimori, T., Gottlieb, E. & Steitz, J. A. The structure of mammalian small nuclear ribonucleoproteins. Identification of multiple protein components reactive with anti-(U1)ribonucleoprotein and anti-Sm autoantibodies. *J. Biol. Chem.* **259**, 5907–5914 (1984).
57. el-Deiry, W. S. *et al.* WAF1, a potential mediator of p53 tumor suppression. *Cell* **75**, 817–825 (1993).
58. Wrana, J. L. *et al.* TGF β signals through a heteromeric protein kinase receptor complex. *Cell* **71**, 1003–1014 (1992).
59. Hata, A., Lo, R. S., Wotton, D., Lagna, G. & Massague, J. Mutations increasing autoinhibition inactivate tumour suppressors Smad2 and Smad4. *Nature* **388**, 82–87 (1997).
60. Feng, X. H. & Derynck, R. Ligand-independent activation of transforming growth factor (TGF) β signalling pathways by heteromeric cytoplasmic domains of TGF-β receptors. *J. Biol. Chem.* **271**, 13123–13129 (1996).
61. Kittler, R. *et al.* Genome-wide resources of endoribonuclease-prepared short interfering RNAs for specific loss-of-function studies. *Nat. Methods* **4**, 337–344 (2007).
62. Lamprecht, M. R., Sabatini, D. M. & Carpenter, A. E. CellProfiler: free, versatile software for automated biological image analysis. *Biotechniques* **42**, 71–75 (2007).
63. Junqueira, M. *et al.* Separating the wheat from the chaff: unbiased filtering of background tandem mass spectra improves protein identification. *J. Proteome Res.* **7**, 3382–3395 (2008).
64. Ong, S. E. & Mann, M. Mass spectrometry-based proteomics turns quantitative. *Nat. Chem. Biol.* **1**, 252–262 (2005).
65. Listerman, I., Bledau, A. S., Grishina, I. & Neugebauer, K. M. Extragenic accumulation of RNA polymerase II enhances transcription by RNA polymerase III. *PLoS Genet.* **3**, e212 (2007).
66. Almeida, F., Saffrich, R., Ansorge, W. & Carmo-Fonseca, M. Microinjection of anti-coilin antibodies affects the structure of coiled bodies. *J. Cell Biol.* **142**, 899–912 (1998).
67. Chaumeil, J., Augui, S., Chow, J. C. & Heard, E. Combined immunofluorescence, RNA fluorescent *in situ* hybridization, and DNA fluorescent *in situ* hybridization to study chromatin changes, transcriptional activity, nuclear organization, and X-chromosome inactivation. *Methods Mol. Biol.* **463**, 297–308 (2008).
68. Bakin, A. & Ofengand, J. Four newly located pseudouridylylated residues in *Escherichia coli* 23S ribosomal RNA are all at the peptidyltransferase center: analysis by the application of a new sequencing technique. *Biochemistry* **32**, 9754–9762 (1993).

DOI: 10.1038/ncb2264

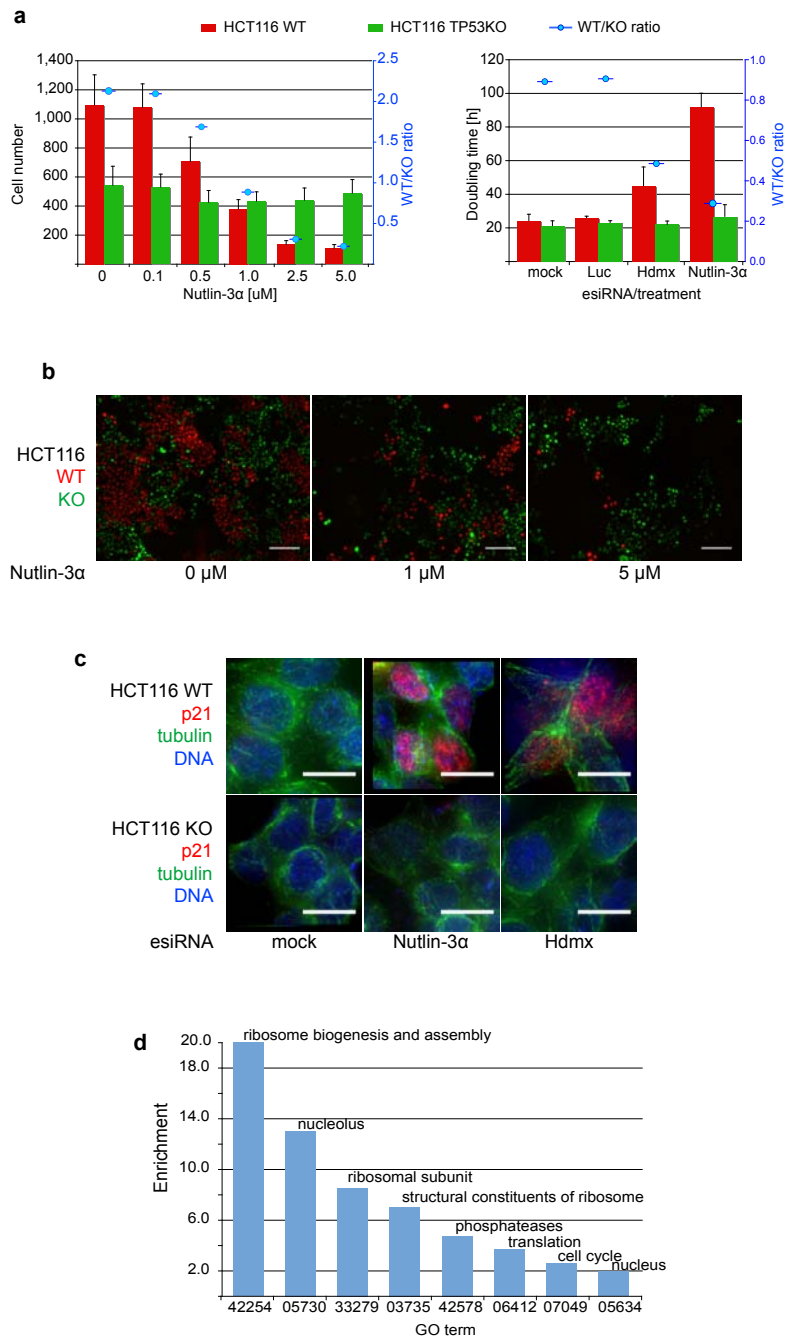


Figure S1 Screening assay evaluation. (a) Left panel – dose-response of WT and KO cell number to different concentrations of Nutlin-3α. WT and KO cells were mixed in 2:1 ratio and grown for 48 hours in the presence of Nutlin-3α. The left y-axis shows the cell number and the right y-axis (blue) represents the WT/KO ratio. Right panel – doubling time of WT and KO cell upon RNAi depletion of control genes or Nutlin-3α treatment (mean±s.d., n = 3). (b) Images of mixed population of WT (red) and KO (green) cells co-cultured in the presence of different concentrations of Nutlin-3α, scale

bar represents distance of 100 μm (mean±s.d., n = 3) (c) Indirect immunofluorescence for p21^{WAF1} protein (red) in WT and KO cells after treatment with 1 mM Nutlin-3α or Hdmx depletion. α-tubulin is stained in green and DNA in blue (DAPI), scale bar represents distance of 10 μm. (d) Gene Ontology terms enrichment analysis of the hits decreasing the WT/KO ratio according to the web-based DAVID bioinformatics resource at the National Institute of Allergy and Infectious Diseases, NIH. Presented are the GO terms with enrichment above 2.

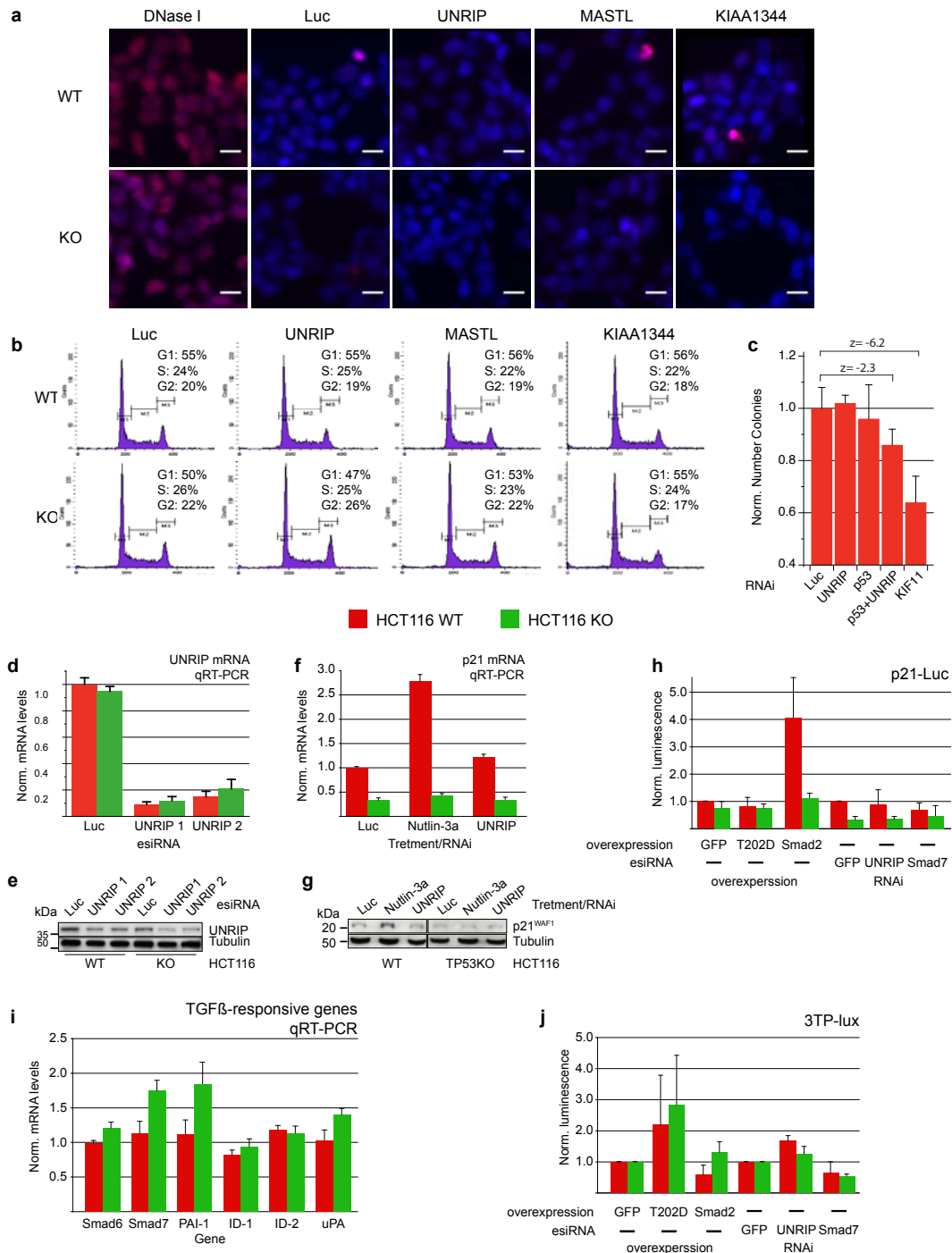


Figure S2 Characterization of the depletion phenotypes of the genes that increase the WT/KO ratio. **(a)** Hits depletion does not lead to apoptosis induction judged by terminal deoxynucleotidyl transferase dUTP nick end labeling (TUNEL) assay (red signal). DNase I treatment shows the robustness of the assay to detect nicked DNA. Scale bars represents distance of 10 μ m. **(b)** Hits depletion does not lead to cell cycle arrest judged by the DNA quantity profiles (propidium iodide staining). **(c)** Colony formation assay in HCT116 WT cells. TP53 and UNRIP co-depletion leads to decreased clonogenic survival (z-score -2.3). KIF11 depletion (z-score -6.2), which gives strong decrease in clonogenic survival, is provided for comparison. Presented is the number of colonies, normalized to luciferase transfection **(d,e)** Quantification of UNRIP mRNA and protein knockdown with two independent esiRNAs. Fold change over control (luciferase)

depletion (mean \pm s.d., n = 3). **(f, g)** Quantification of p21/WAF1 mRNA and protein levels upon UNRIP knockdown. The fold change is calculated over luciferase knockdown in the WT cells (mean \pm s.d, n = 3). Treatment with 1 mM Nutlin-3a for 24 hours is used as a control of p53 activation. **(h)** p21^{WAF1}-luc reporter induction upon TGF β signaling activation (overexpression of T202D, Smad2) or depletion (UNRIP, Smad7). The values are normalized to GFP overexpression or depletion, respectively. **(i)** Quantitative RT-PCR analysis of TGF β responsive genes upon UNRIP depletion. Fold change over control (luciferase) depletion (mean \pm s.d., n = 3). **(j)** 3TP-luc reporter induction upon TGF β signaling activation (overexpression of T202D, Smad2) or depletion (UNRIP, Smad7). The values are normalized to negative controls GFP overexpression or depletion, respectively (mean \pm s.d., n = 3).

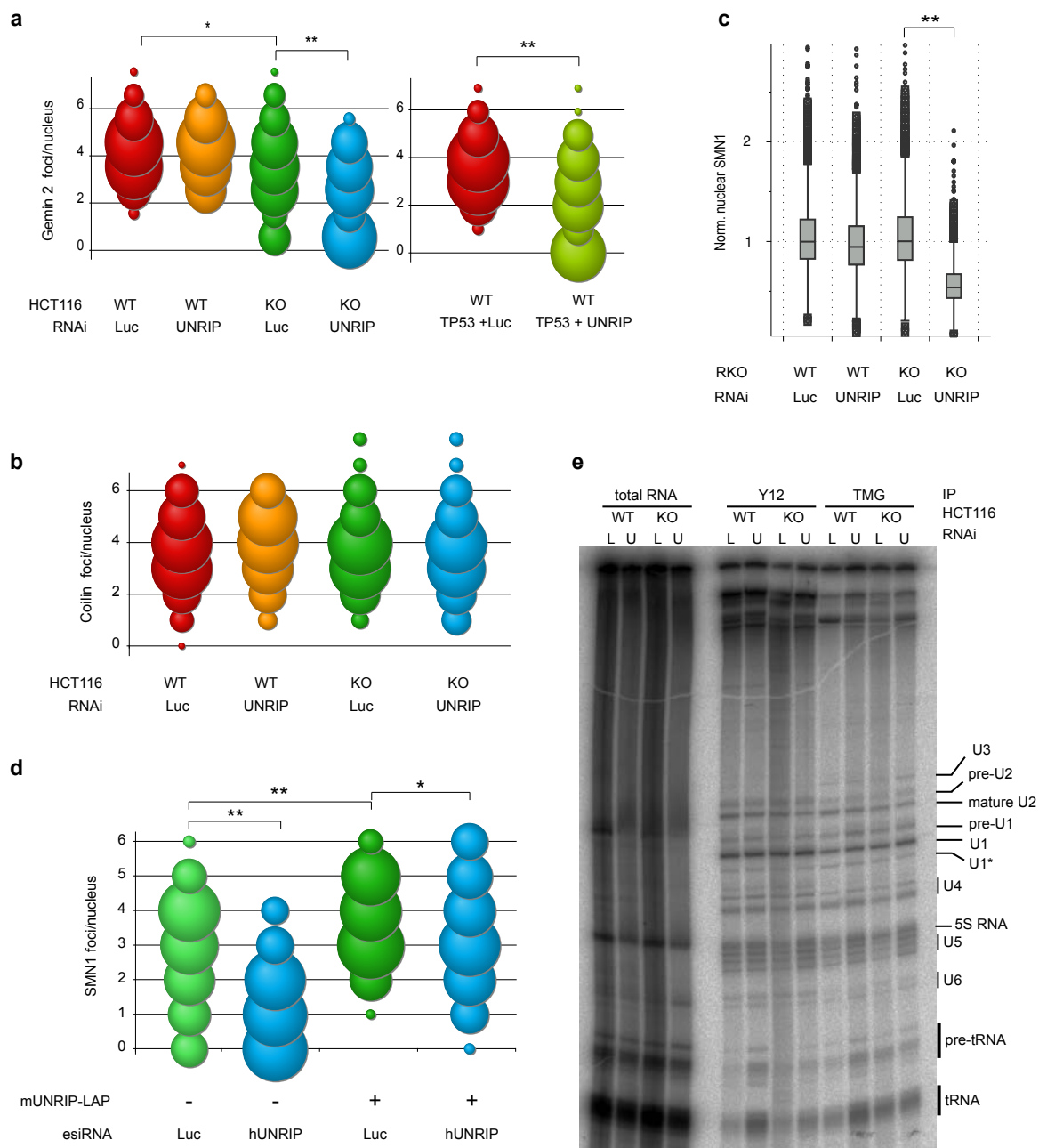


Figure S3 UNRIP depletion influences SMN complex localization but not snRNAP assembly activity. Quantification of Gemin2 (a) and p80/Coilin (b) foci per nucleus upon UNRIP depletion. The sizes of the balls represent the percentage of the cells with the corresponding number of foci. The *p*-values were calculated with two-tailed *t*-test, * - *p*-values < 0.01, ** - *p*-values < 10⁻⁵, counted 200-300 nuclei per condition in three independent experiments. (c) Box plot showing the amount of nuclear SMN1, determined by immunofluorescent staining, in RKO cells upon UNRIP depletion. The

median of luciferase depleted RKO WT cells is normalized to 1. The *p*-values were calculated with two-tailed *t*-test, ** - *p*-values < 0.01. (d) Expression of mouse UNRIP-LAP in HCT116 KO cells rescues SMN1's localization to the CB upon depletion of the endogenous human UNRIP. (e) UNRIP is dispensable for the snRNP assembly *in vivo*. HCT116 cells were UNRIP depleted (L - luciferase, U - UNRIP), ³²P-orthophosphate metabolically labeled and snRNPs, immunoprecipitated with anti-Sm (Y12) or anti-TMG antibody, were analyzed on a denaturing AA-PAGE. U1* - degradation product of U1 snRNA.

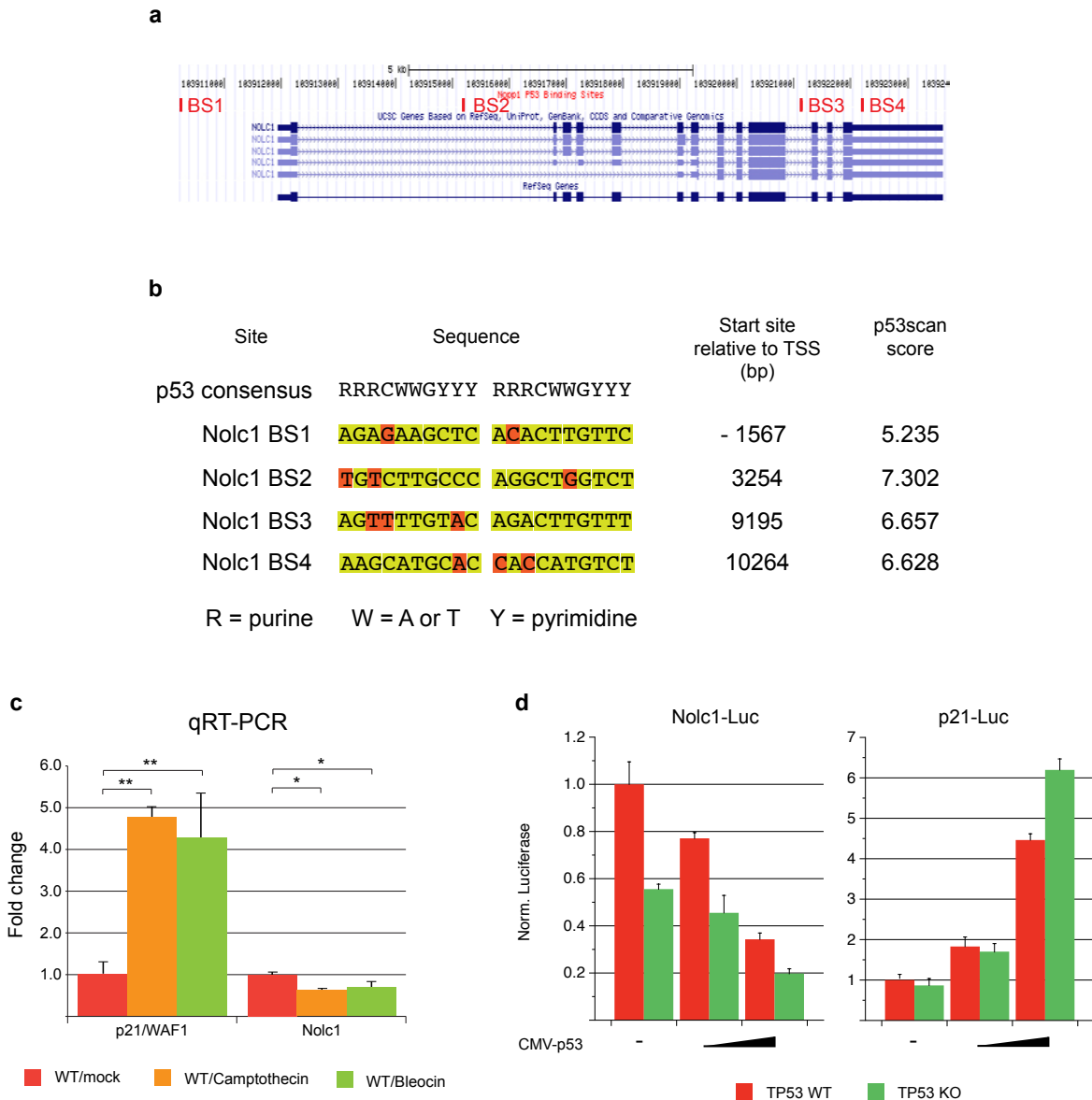


Figure S4 Description of p53 binding sites in *Nolc1* gene. (a) The positions of the putative p53 binding sites (BS from 1 to 4) in *Nolc1* gene are represented as red bars on a UCSC Genome Browser (Feb.2009 Assembly) depiction of the *Nolc1* genomic sequence. (b) Sequence information about the putative p53 binding sites. The mismatches with the consensus p53 binding sequence¹ and are highlighted in red. Shown are the distances (in base pairs) from the transcription start site (TSS). p53scan score is calculated with the following parameters: spacer length $s=0-1$, cutoff c

4.39 and 13.7 for $s=0$ and $s=1$ respectively, number of returned results $n=5$ as described². (c) Quantitative RT-PCR analysis of *p21/WAF1* and *Nolc1* mRNA in HCT116 WT cells after treatment with 5 mM camptothecin or 0.5 mg/ml bleocin for 4 hours. The values are normalized to DMSO treated control, t -test p -values are denoted as * - $p < 0.05$ and ** - $p < 0.001$ (mean \pm s.d., $n=3$). (d) Response of *Nolc1* and *p21* promoter carrying luciferase reporter constructs to p53 WT overexpression in HCT116 WT and KO cells (mean \pm s.d., $n=3$).

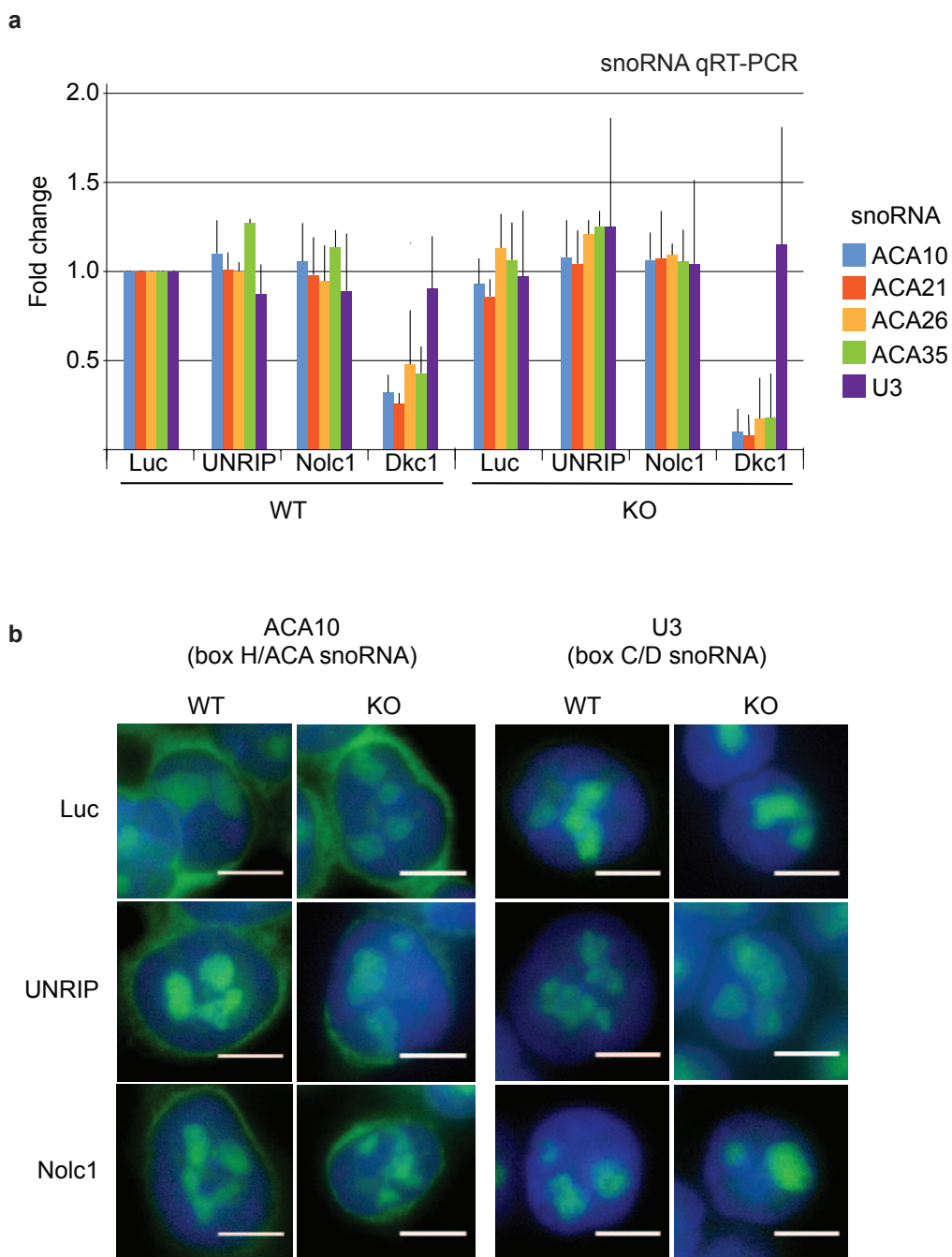


Figure S5 Nolz1 and UNRIP do not play a role in snoRNA stability and trafficking. **(a)** Quantification of the levels of five mature snoRNAs upon Nolz1, UNRIP or Dkc1 depletion in WT and KO cells. The values are normalized to

Luc depleted WT cells (mean \pm s.d., n = 3). **(b)** RNA FISH shows the cellular localization of representative box H/ACA (ACA10) and box C/D (U3) snoRNAs upon UNRIP or Nolz1 depletion. Scale bar represents distance of 5 μ m.

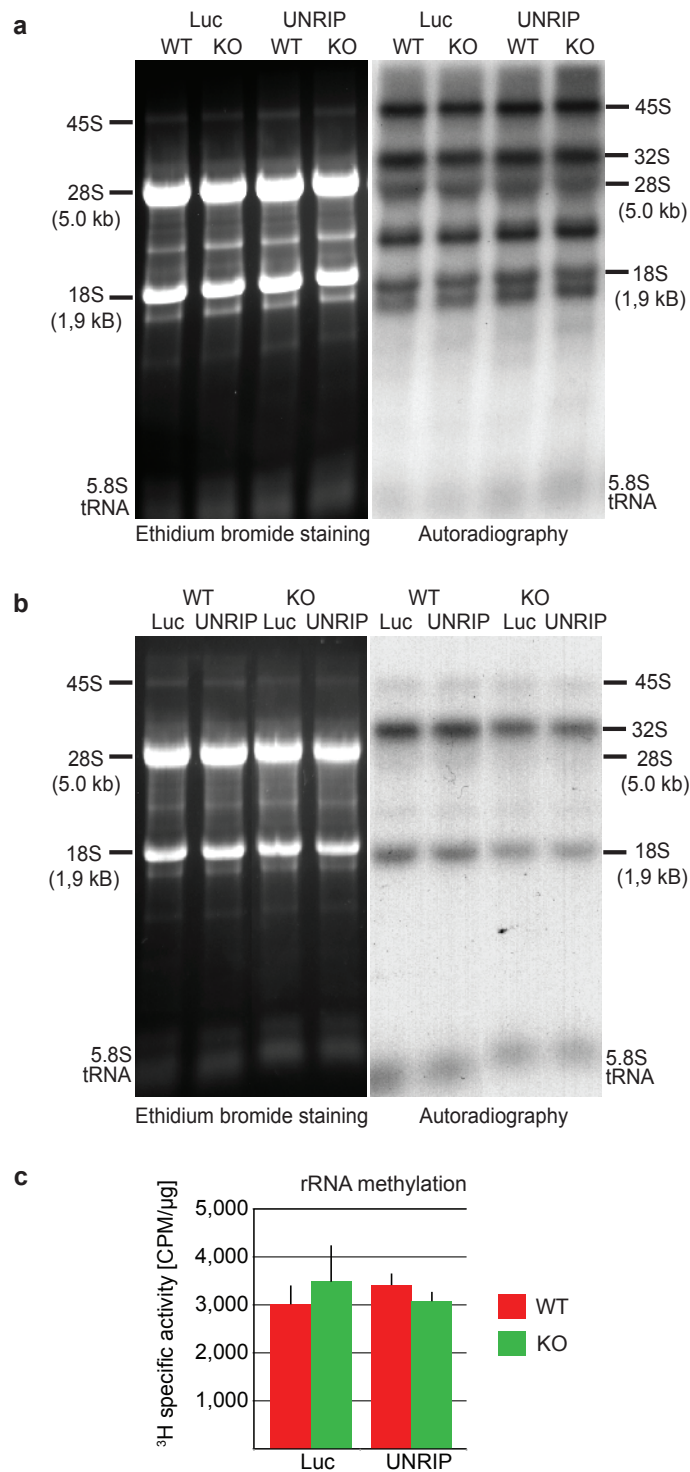


Figure S6 rRNA cleavage maturation and methylation are not affected by Nolc1 and UNRIP. (a) rRNA cleavage patterns were investigated in UNRIP depleted ³²P-orthophosphate metabolically labeled cells. After 30 min chase period, 5 μg total RNA were resolved on a denaturing agarose gel and autoradiographed. (b) rRNA methylation was investigated in UNRIP

depleted L-[methyl-³H]-Methionine metabolically labeled cells. After 30 min chase period, 5 μg total RNA were resolved on a denaturing agarose gel and autoradiographed. (c) Quantification of the incorporation of methyl groups in the rRNA, ³H specific activity, measured on a scintillation counter.

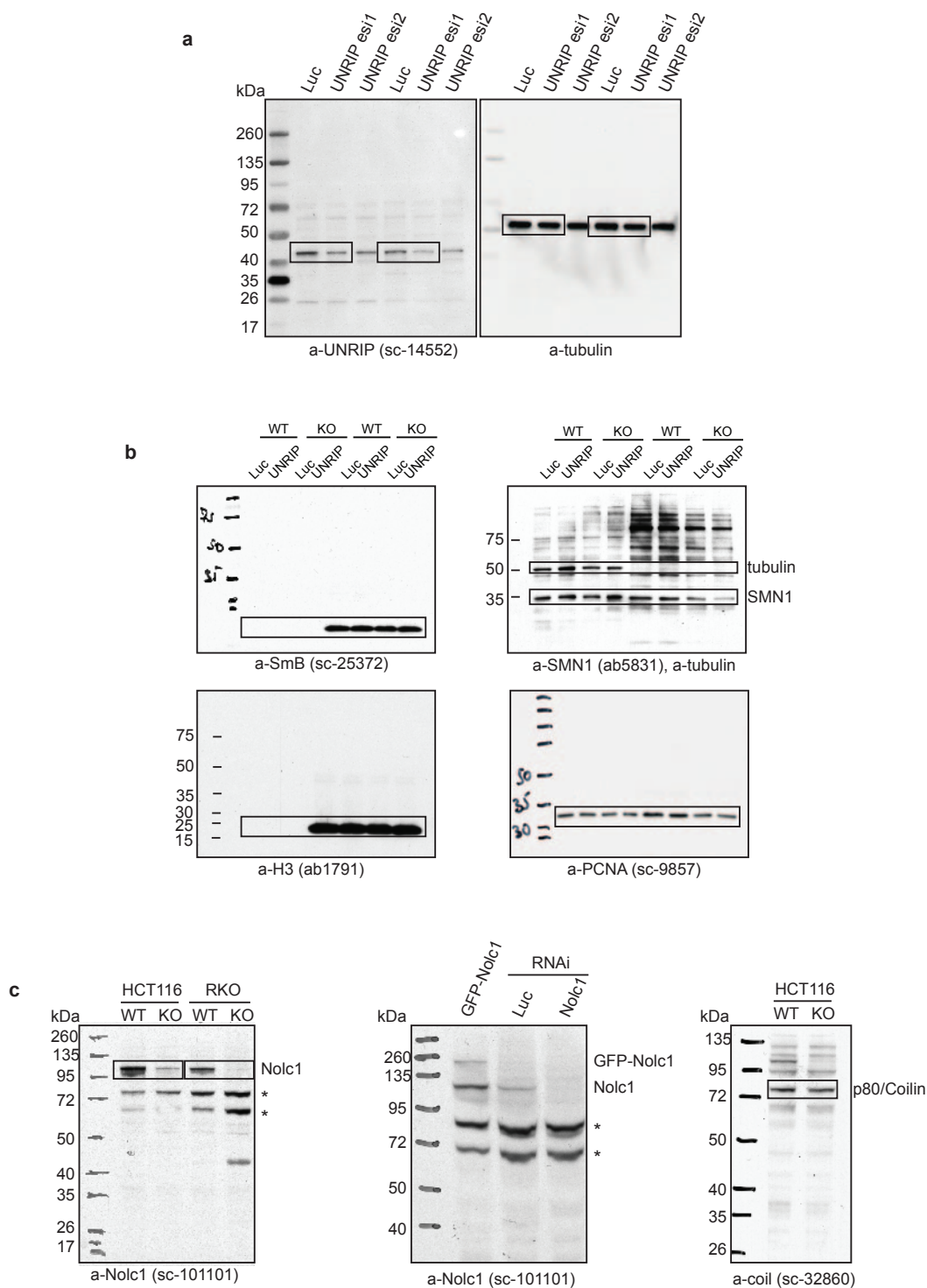


Figure S7 Full scans of blots. (a) Uncropped scans of UNRIP knockdown, Fig.2d and Fig. S2e. (b) Uncropped scans of the blots on Fig. 3c. (c)

Uncropped scans of the blots on Fig. 4c, * - unspecific bands (they cannot be depleted by RNAi and cannot be shifted by GFP-tagging).

Table S1 Genome-scale screen primary data and calculated scores. A and B in the column names denote values obtained from the technical replicates of the screen.

Table S2 Validated screen hits with their scores and primers for esiRNA generation.

Table S3 Summary of MS analysis of UNRIP-LAP complexes. The 'Recovery' column summarizes how many times a protein was identified in total of 7 independent pulldown purifications.

Table S4 Primers used in the study.

Supplementary References

1. Riley, T., Sontag, E., Chen, P. & Levine, A. Transcriptional control of human p53-regulated genes. *Nat Rev Mol Cell Biol* 9, 402-412 (2008).
2. Smeenk, L. *et al.* Characterization of genome-wide p53-binding sites upon stress response. *Nucleic Acids Res*, 17 (2008).
3. Mattia, M. *et al.* p53-dependent p21 mRNA elongation is impaired when DNA replication is stalled. *Mol Cell Biol*, 27 (2007).